



# Metal source and ore-forming process of the Maoping carbonate-hosted Pb-Zn deposit in Yunnan, SW China: Evidence from deposit geology and sphalerite Pb-Zn-Cd isotopes

Tao Wu <sup>a,b</sup>, Zhilong Huang <sup>a,\*</sup>, Yufan He <sup>c</sup>, Mu Yang <sup>d</sup>, Haifeng Fan <sup>a</sup>, Chen Wei <sup>a,b</sup>, Lin Ye <sup>a</sup>, Yusi Hu <sup>a,b</sup>, Zhenzhong Xiang <sup>a,b</sup>, Chunkit Lai <sup>e</sup>

<sup>a</sup> State Key Laboratory of Ore Deposit Geochemistry, Institute of Geochemistry, Chinese Academy of Sciences, Guiyang 550081, China

<sup>b</sup> University of Chinese Academy of Sciences, Beijing 100049, China

<sup>c</sup> School of Management, Guizhou University of Commerce, Guiyang 550081, China

<sup>d</sup> School of Geoscience and Info-Physics, Central South University, Changsha 410083, China

<sup>e</sup> Faculty of Science, Universiti Brunei Darussalam, Gadong BE1410, Brunei Darussalam

## ARTICLE INFO

### Keywords:

Sphalerite Pb-Zn-Cd isotopes

Maoping Pb-Zn deposit

Ore metal source

Fluid mixing

Mississippi Valley-type (MVT)

## ABSTRACT

The Maoping carbonate-hosted Pb-Zn deposit (25 Mt ores @ 12–35% Zn + Pb) is a representative and the third-largest Pb-Zn deposit in the Sichuan-Yunnan-Guizhou Pb-Zn metallogenic province (SYGMP). In this study, Pb-Zn-Cd isotope analyses were performed on sphalerite from Maoping, in order to understand the ore metal source and metallogenesis in the SYGMP. The sphalerite samples have narrow ranges of Pb isotope ratios:  $^{206}\text{Pb}/^{204}\text{Pb} = 18.675\text{--}18.751$ ,  $^{207}\text{Pb}/^{204}\text{Pb} = 15.758\text{--}15.768$ , and  $^{208}\text{Pb}/^{204}\text{Pb} = 39.287\text{--}38.436$ . This implies thorough mixing of two Pb sources, which we interpreted to be the Devonian-Carboniferous ore-hosting carbonate wall-rocks and the Neoproterozoic Kunyang/Huili Group (Gp.) clastic and metamorphic rocks. The Maoping sphalerite samples have uniform  $\delta^{66}\text{Zn}$  ( $-80.07 \pm 0.25\text{\textperthousand}$ ) and  $\delta^{114}\text{Cd}$  ( $-0.10 \pm 0.27\text{\textperthousand}$ ) values, which further support complete source mixing. In the  $\delta^{66}\text{Zn}$  vs. Cd/Zn plot, the Maoping sphalerite data fall close to the field of basement rocks and distal to the carbonate wallrocks, indicating that the ore zinc was mainly derived from the metamorphic basement with heavier  $\delta^{66}\text{Zn}$  values and low Cd/Zn ratios with certain contributions from the minor carbonate wallrock with lower  $\delta^{66}\text{Zn}$  values and high Cd/Zn ratios. In the  $\delta^{114}\text{Cd}$  vs. 1/Cd plot, all Maoping sphalerite samples fall inside the Mississippi Valley-type (MVT) field, and the deposit shares many geological and sulfide geochemical (incl. isotopic) features with MVT deposits. Thus, the Maoping Pb-Zn mineralization is best classified as MVT, and the sulfide precipitation in structural (fault-fold) traps was caused by binary mixing of a metal-bearing and a reduced S-bearing fluid.

## 1. Introduction

The world-class Sichuan-Yunnan-Guizhou metallogenic province (SYGMP) in South China hosts ~ 400 Pb-Zn deposits, containing a total of > 200 Mt ores @ 10–15% Pb + Zn (Fig. 1a; Liu and Lin, 1999; Huang et al., 2004, 2011; Hu et al., 2017). During the past two decades, many studies were conducted on the SYGMP carbonate-hosted Pb-Zn deposits, especially on their geological features and mineralization ages (e.g., Huang et al., 2004; Li et al., 2004; Han et al., 2007; He et al., 2017; Zhou et al., 2013a, 2013b, 2015, 2018b; Xu et al., 2019). Despite these

studies, the regional Pb-Zn ore metal source has been variably attributed to the Emeishan flood basalt, the metamorphic basement, and/or the Sinian-Permian sedimentary sequences (e.g., Huang et al., 2004; Zhou et al., 2013a, 2013b, 2018b; Zhu et al., 2013, 2018; Luo et al., 2019; Xiang et al., 2020 and reference therein). The lack of ore metal source constraints limits the construction of an inclusive regional Pb-Zn metallogenic model.

The large Maoping Pb-Zn deposit (>3.0 Mt contained Zn + Pb; Wei et al., 2015; Xiang et al., 2020) is typical in the SYGMP, and is hosted by Devonian-Carboniferous carbonate rocks (Zhang et al., 2015).

\* Corresponding author.

E-mail addresses: [wutao@mail.gyig.ac.cn](mailto:wutao@mail.gyig.ac.cn) (T. Wu), [huangzhihong@vip.gyig.ac.cn](mailto:huangzhihong@vip.gyig.ac.cn) (Z. Huang), [beliefhyf@foxmail.com](mailto:beliefhyf@foxmail.com) (Y. He), [yangmu@csu.edu.cn](mailto:yangmu@csu.edu.cn) (M. Yang), [fanhafeng@mail.gyig.ac.cn](mailto:fanhafeng@mail.gyig.ac.cn) (H. Fan), [weichen@mail.gyig.ac.cn](mailto:weichen@mail.gyig.ac.cn) (C. Wei), [yelin@vip.gyig.ac.cn](mailto:yelin@vip.gyig.ac.cn) (L. Ye), [huyusi@mail.gyig.ac.cn](mailto:huyusi@mail.gyig.ac.cn) (Y. Hu), [472379780@qq.com](mailto:472379780@qq.com) (Z. Xiang), [chunkitl@utas.edu.au](mailto:chunkitl@utas.edu.au) (C. Lai).

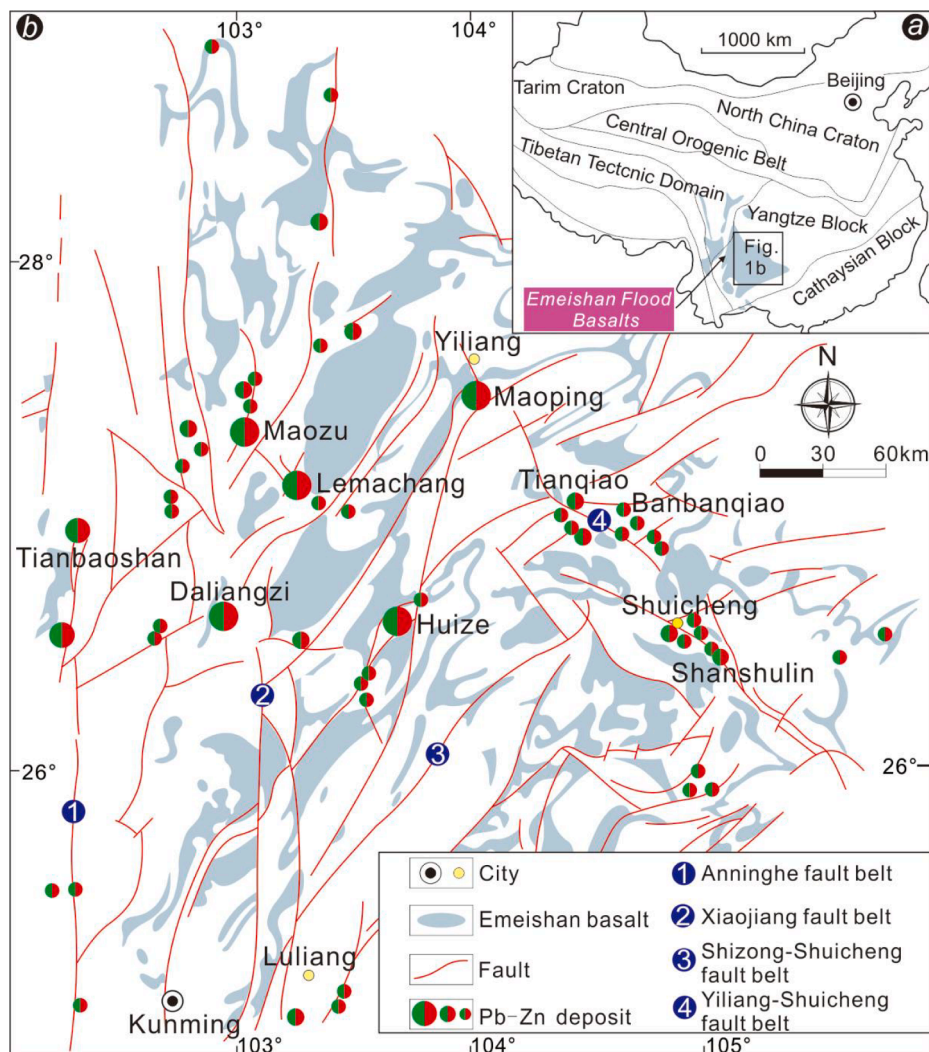


**Fig. 1.** (a) Tectonic map of China, showing the location of the Sichuan-Yunnan-Guizhou (SYG) region and Emeishan Large Igneous Province (ELIP) (modified after He et al., 2020). (b) Regional geologic map of the SYG Pb-Zn mineral province, showing the distribution of Emeishan flood basalts, major structures, and Pb-Zn deposits (modified from Liu and Lin, 1999).

Previously, Han et al. (2007) suggested that the ore fluids were of medium temperatures (180–280 °C) and low salinities (4.1–9.5 wt% NaCl equiv.). Yang et al. (2019) reported a Late Triassic mineralization age by sphalerite Rb-Sr dating ( $202.5 \pm 8.5$  Ma), possibly related to the late Indosinian orogeny. Certain studies suggested that the reduced sulfur was sourced from marine evaporite in the ore-bearing sequence, via thermochemical (TSR) and/or bacteria sulfate reduction (BSR) (Ren et al., 2018; Tan et al., 2019; He et al., 2020; Xiang et al., 2020). As for the metal source(s), some authors proposed that the ore metals were sourced mainly from the carbonate ore host (Tan et al., 2019; Xiang et al., 2020), whereas He et al. (2020) suggested a mixed source from the ore-bearing carbonate and basement rocks, in addition to minor contribution from the Emeishan flood basalt. In terms of the deposit type, the Maoping was variably proposed to be sedimentary-reworking (Liu and Lin 1999), SEDEX (Wang et al. 2009), or MVT (He et al., 2020; Wei et al., 2021) type.

Recent advances in multi-collector inductively coupled plasma mass spectrometer (MC-ICP-MS) enable high-precision measurement of transition metal isotopes (e.g., Zn, Cd) with good long-term reproducibility (below  $\pm 0.06\%$  for Zn and Cd isotopes; Zhu et al., 2020), opening a new opportunity to better understand various metallogenic processes (e.g., Wilkinson et al., 2005; Moynier et al., 2017; Zhu et al., 2018, and

reference therein). Due to their high abundance in typical Pb-Zn deposits, Zn and Cd isotopes are considered as good tracer for ore-metal source and ore-forming processes (Mason et al., 2005; John et al., 2008; Kelley et al., 2009; Pašava et al., 2014; Zhou et al., 2014a; Zhu et al., 2013, 2018). For example, based on sphalerite Zn isotope study, Kelley et al. (2009) proposed a mixing model of a metal-bearing and a sulfur-bearing fluid for the Red Dog shale-hosted massive sulfide deposits in NW Alaska (USA).

In this study, we integrated unconventional Zn-Cd isotopes with conventional Pb isotope MC-ICP-MS analyses on the Maoping ore sphalerite, in order to constrain the ore metal source(s) and possible metallogenic implications from the Zn-Cd isotope variation. Our findings provide a new insight into the carbonate-hosted Pb-Zn metallogeny in the SYGMP.

## 2. Geological setting

### 2.1. Regional geology

In the Neoproterozoic (ca. 820–850 Ma), the Yangtze block collided with the Cathaysia block along the Jiangnan orogen to form the South China block (e.g., Zhao et al. 2010). Subsequently, the South China block

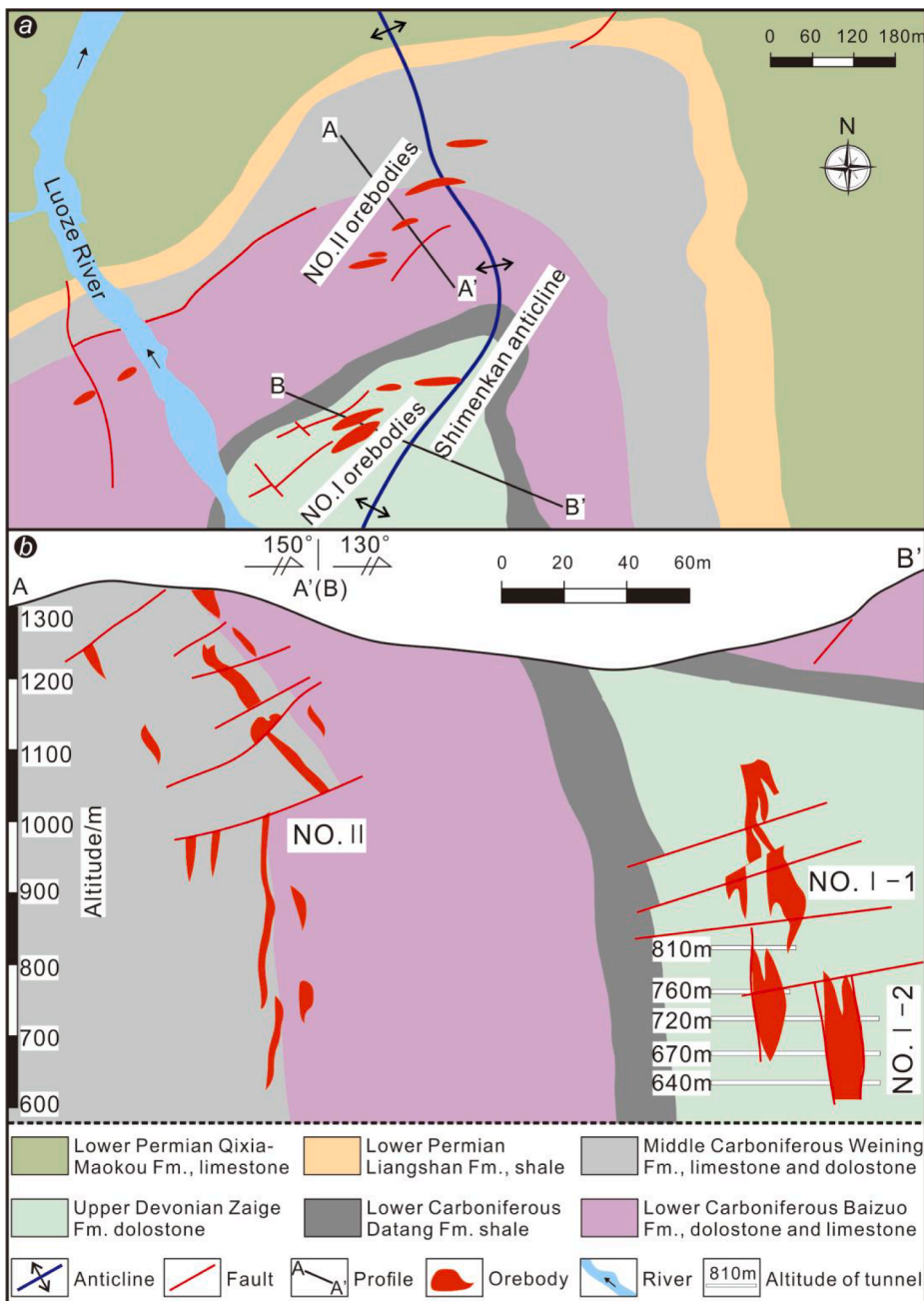


**Fig. 2.** (a) Geological sketch map of the Maoping Pb-Zn deposit, showing the distribution of the sedimentary sequences, structures (fold and fault), orebodies, and the A-A'-B-B' profile location (modified from Liu and Lin, 1999; Wei et al., 2015). (b) Geological cross-section of the Maoping A-A'-B-B' profile, showing the distributions of Pb-Zn orebodies and lithologic units (modified after Wei et al., 2015).

collided in the Triassic with the North China and Indochina block to its north and southwest, respectively (e.g., Wang et al., 2013). The Sichuan-Yunnan-Guizhou (SYG) district in the southwestern Yangtze block (Fig. 1a) is confined by three regional fault zones, i.e., the Anninghe (NS-trending), Yiliang-Shuicheng (NW-trending), and Shizong-Shuicheng (NE-trending) (Fig. 1b; Ren et al., 2018; He et al., 2020). The western Yangtze block contains a basement consisting of Archean (ca. 3.3–2.9 Ga), Paleo-proterozoic (ca. 2.5–2.1 Ga), Mesoproterozoic (ca. 1.7–1.5 Ga; Dongchuan Group (Gp.)), and Neoproterozoic (ca. 1.1–0.9 Ga; Kunyang/Huili Gp.) metamorphic rocks (Zhao et al., 2010; Gao et al., 2011; Qiu et al., 2016; Xiang et al., 2020). The folded basement rocks, including mainly slate and metamorphosed greywacke-carbonate-tuff interbeds, are widely exposed in the SYG region (Yan et al., 2003; Hu et al., 2017; Zhou et al., 2018a).

Overlying the basement are the Ediacaran-Triassic marine carbonate and clastic sedimentary rocks, Late Permian Emeishan continental flood basalts, and Jurassic-Quaternary continental sedimentary rocks (Liu and Lin, 1999; Zhang et al., 2019a; Xiang et al., 2020). The mantle plume-related Emeishan basalts (~260 Ma) cover > 250,000 km<sup>2</sup> in the southwestern Yangtze block (Fig. 1a; Zhou et al., 2002), and are spatially associated with the SYG carbonate-hosted Pb-Zn mineralization. Sphalerite Rb-Sr and calcite/fluorite Sm-Nd dating showed that these deposits were mainly formed in ca. 225–192 Ma, interpreted to have linked to the *syn-collision* compression and post-collisional extension of the Indosinian Orogeny (Li et al., 2004; Li et al., 2007; Lin et al., 2010; Hu and Zhou, 2012; Zhou et al., 2013b, 2015; Zhang et al., 2015; Zhou et al., 2018a; Yang et al., 2019).

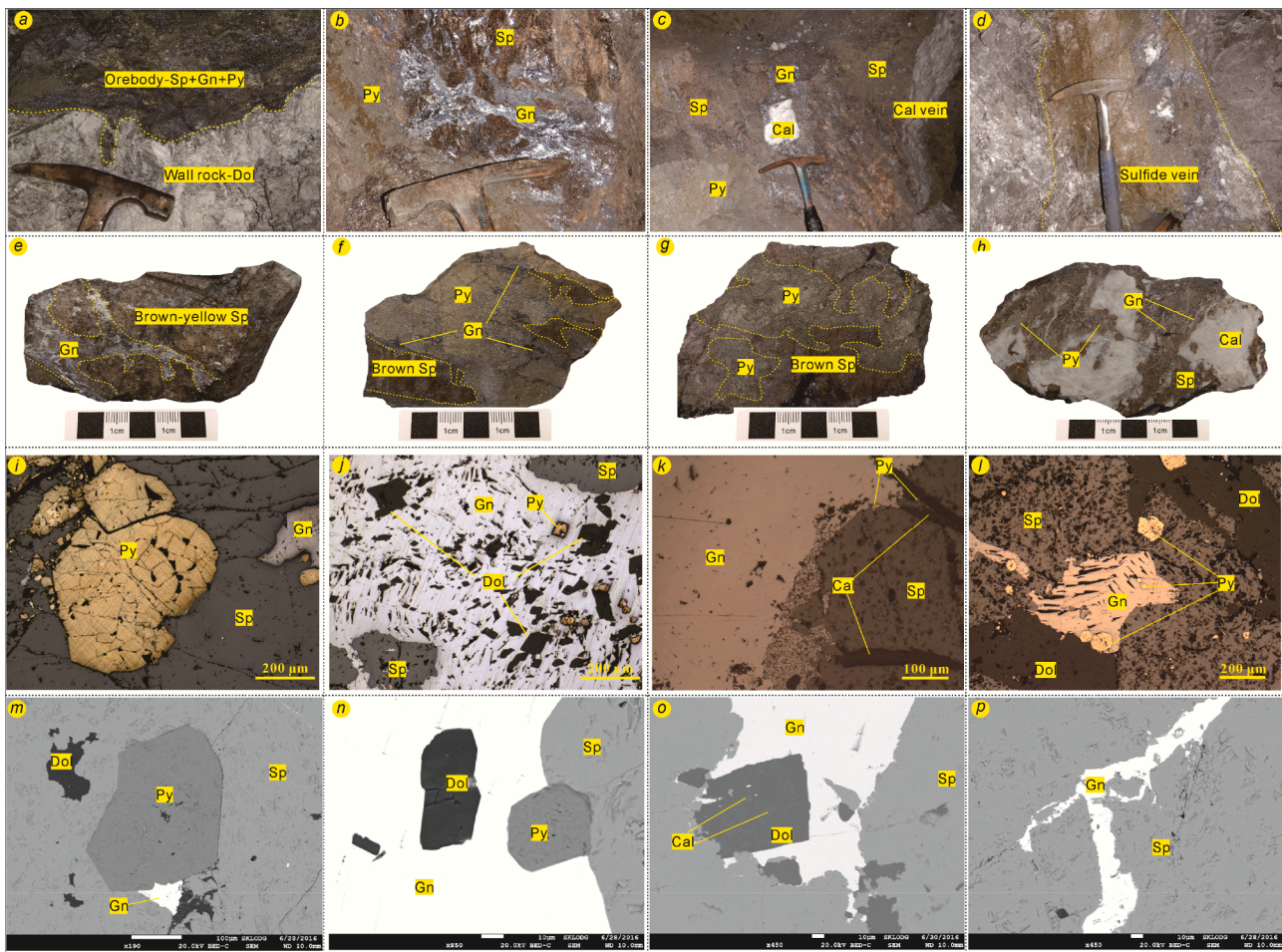


**Fig. 3.** Field (a–d), hand-specimen (e–h), microscope (g–i) photographs and SEM images (m–p) of the occurrence and textures of sulfide ore at Maoping: (a) Clear boundary between sulfide orebody and wallrocks. (b) Massive sphalerite and galena enclosed by pyrite. (c) Massive sulfide orebody cut by late calcite vein. (d) Sulfide vein as wallrock fracture infill. (e) Brown-yellow sphalerite replaced by galena stockwork. (f) Pyrite-sphalerite-galena ore mineral assemblage. (g) Brown sphalerite replaced the early-formed pyrite. (h) Brecciated sulfides ores. (i) Euhedral pyrite enclosed by late sphalerite. (j) Anhedral sphalerite and fine-grained pyrite replaced by late galena. (k) Coarse-grained sphalerite replaced by galena. (l) Porous sphalerite overgrowth with pyrite and galena. (m) Euhedral pyrite enclosed by late sphalerite. (n) Euhedral pyrite distributed along the boundary of sphalerite and galena. (o) Galena and dolomite as void-infill in early sphalerite. (p) Galena veinlet cut early sphalerite. Abbreviations: Gn—galena; Sp—sphalerite; Py—pyrite; Cal—calcite; Dol—dolomite.

## 2.2. Deposit geology

The Maoping Pb-Zn mining district (in the northeastern SYGMP; Fig. 1b) is located in the tectonic junction of the regional NE-trending Yadu-Ziyun and Zhaotong-Qujing faults (Tan et al., 2019). Local stratigraphy (mainly Devonian to Permian) comprises the Upper Devonian Zaige Fm. dolostone and sandstone-mudstone. These are in turn overlain by the Lower Carboniferous Datang Fm. limestone (with thin shale beds) and Baizuo Fm. dolostone-shale interbeds. The Middle Carboniferous Weining Formation above mainly consists of limestone and dolostone, which is overlain successively by the Lower Permian Liangshan Fm. shale-sandstone and the Lower Permian Qixia and Maokou Fms. limestone. The Emeishan flood basalts are widespread outside the mining area (Fig. 2a).

Distribution of the Pb-Zn orebodies is structurally controlled by the Shimenkan inverted anticline (dominant), the NE-trending Maoping fault, and its secondary interlayer fractures (Fig. 2a-b, 3a; Wei et al., 2015). The Shimenkan inverted anticline has its fold axis striking NE $20^{\circ}$ – $45^{\circ}$  in the north and NW $350^{\circ}$  in the west. The western limb is overturned with a dip angle of  $65^{\circ}$ – $86^{\circ}$ , while the eastern limb has a relatively gentle dip ( $17^{\circ}$ – $35^{\circ}$ ). The Maoping fault (30 km) long strikes NE $10^{\circ}$ – $80^{\circ}$  and dips SE $65^{\circ}$ – $85^{\circ}$ .

Orebodies at Maoping occur as steeply-plunging pipes (Fig. 2b) and fall into two groups (Gp. I-II; Fig. 2a, b; He et al., 2020). Group I orebodies are hosted in the Upper Devonian Zaige Formation, accounting for 70% of the total metal reserve at Maoping (Wei et al., 2015). These orebodies are 280–320 m long, 5.0–31.0 m thick, and have average grade of 12.8% Zn and 5.5% Pb. Group II orebodies are developed in the interlayer fractures of the Carboniferous Baizuo-Weining formations. These orebodies are 40–150 m long, 0.2–6.0 m thick, and have average grade of 13.6% Zn and 2.8% Pb.

The Maoping Pb-Zn ores are chiefly of open-space-filling and replacement types (Fig. 3a–h), and comprise mainly sulfides with minor oxides. Sulfide ore textures include massive (Fig. 3a, c, g), brecciated (Fig. 3b, h), and veined (Fig. 3d). Metallic minerals include sphalerite, galena, and pyrite, whilst non-metallic minerals include mainly dolomite and calcite and minor quartz (Fig. 3). Ore minerals are subhedral-anhedral granular (Fig. 3i, j, m–o), or have metasomatic (Fig. 3j–l, n, o), enclosed (Fig. 3i, j, m–o), crosscutting vein (Fig. 3p), and coplanar (Fig. 3m–o) textures.

**Table 1**

Lead isotope compositions of sphalerites from the Maoping No. I-1 and No. I-2 orebodies.

Sample	Location	Oreboddy	$^{208}\text{Pb}/^{204}\text{Pb}$	$\pm 2\sigma$	$^{207}\text{Pb}/^{204}\text{Pb}$	$\pm 2\sigma$	$^{206}\text{Pb}/^{204}\text{Pb}$	$\pm 2\sigma$
MP-16-7	760 m	I-1	39.428	0.001	15.767	0.001	18.744	0.001
MP-16-8	760 m	I-1	39.431	0.002	15.767	0.001	18.746	0.001
MP-16-9	760 m	I-1	39.428	0.001	15.768	0.001	18.751	0.001
MP-16-14	760 m	I-1	39.436	0.002	15.768	0.001	18.751	0.001
MP-16-15	760 m	I-1	39.434	0.002	15.767	0.001	18.747	0.001
MP-16-16	760 m	I-1	39.414	0.001	15.765	0.001	18.738	0.001
MP-16-17	760 m	I-1	39.381	0.002	15.764	0.001	18.725	0.001
MP-16-18	760 m	I-1	39.411	0.002	15.767	0.001	18.737	0.001
MP-16-22	760 m	I-1	39.394	0.002	15.765	0.001	18.730	0.001
MP-16-37-1	720 m	I-1	39.393	0.002	15.765	0.001	18.728	0.001
MP-16-37-2	720 m	I-1	39.393	0.002	15.766	0.001	18.726	0.001
MP-16-70	720 m	I-2	39.358	0.002	15.765	0.001	18.705	0.001
MP-16-72	720 m	I-2	39.425	0.002	15.766	0.001	18.744	0.001
MP-16-73	720 m	I-2	39.355	0.002	15.765	0.001	18.705	0.001
MP-16-75	720 m	I-2	39.331	0.002	15.763	0.001	18.693	0.001
MP-16-82	720 m	I-2	39.337	0.004	15.762	0.002	18.696	0.002
MP-16-86	720 m	I-2	39.392	0.002	15.765	0.001	18.732	0.001
MP-16-87	720 m	I-2	39.288	0.002	15.761	0.001	18.678	0.001
MP-16-40	670 m	I-2	39.407	0.002	15.767	0.001	18.736	0.001
MP-16-41	670 m	I-2	39.401	0.001	15.765	0.001	18.732	0.001
MP-16-45	670 m	I-2	39.370	0.002	15.766	0.001	18.713	0.001
MP-16-49	670 m	I-2	39.370	0.002	15.764	0.001	18.713	0.001
MP-16-54	640 m	I-2	39.287	0.005	15.758	0.002	18.675	0.002
MP-16-58	640 m	I-2	39.436	0.002	15.768	0.001	18.748	0.001
MP-16-61-1	640 m	I-2	39.385	0.006	15.760	0.002	18.727	0.002
MP-16-61-2	640 m	I-2	39.426	0.005	15.768	0.002	18.743	0.002

### 3. Sampling and analytical methods

#### 3.1. Sampling

In this study, sulfide ore samples at Maoping were collected from the 760 m, 720 m, 670 m, and 640 m adits of the No. I orebody (Fig. 2), the only operating orebody in the mine. Dark (brown) and light (brownish-yellow and light-yellow) pure sphalerite (40–60 mesh) were handpicked from the crushed sulfide samples under a binocular microscope. Representative sphalerite samples were selected for the subsequent Pb ( $n = 26$ ), Zn ( $n = 23$ ), and Cd ( $n = 21$ ) isotope analyses. The sampling location and other sampling information were listed in Tables 1 and 2.

#### 3.2. Methods

All the analyses in this study were carried out at the State Key Laboratory of Ore Deposit Geochemistry (SKLODG), Institute of Geochemistry Chinese Academy of Science (IGCAS). Scanning electron microscope (SEM) images were obtained using a JSM7800F (JEOL, Japan) SEM equipped with a TEAM Apex XL (EDAX, America) energy dispersive X-ray spectrometer (EDS). The beam current used was 10 nA with 25 kV accelerating voltage, and 200  $\times$  magnification was used for most images. Back-scattered electron (BSE) images were obtained for the ore minerals.

The sphalerite Zn-Cd contents were measured with a Varian Vista MPX inductively coupled plasma optical emission spectrometer (ICP-OES). The Pb, Zn and Cd separation was performed at the clean laboratory of the SKLODG, with the detailed procedures as described by Zhu et al. (2016), Zhu et al. (2018). Before the Pb, Zn and Cd isotope analyses, 3 ml AGMP-1 anion-exchange resin (100–200 mesh; BIO-RAD, USA) was used to chemically purify the Pb, Zn and Cd in the sphalerite samples (Tang et al., 2006).

The isotope analyses were conducted on a Thermo Scientific Neptune Plus MC-ICP-MS instrument, following the procedures described by He et al. (2016) and Zhu et al. (2018). For the Pb isotope analysis, the samples were doped with Tl to facilitate instrumental mass bias correction, based on an exponential mass law dependence. NIST NBS-981 ( $^{206}\text{Pb}/^{204}\text{Pb} = 16.9405$ ,  $^{207}\text{Pb}/^{204}\text{Pb} = 15.4963$ ,  $^{208}\text{Pb}/^{204}\text{Pb} = 36.7219$ ; Yuan et al., 2016) was used as the external standard.

For the Zn and Cd isotope analyses, the sample-standard bracketing (SSB) method was used to correct instrumental drift and mass bias (e.g., Zhu et al., 2002). The internal IRMM 3702 and secondary NIST SRM 683 reference standards were used for the Zn isotope measurement. The sample  $\delta^{66}/^{64}\text{Zn}$  values (relative to IRMM 3702) were calculated with the formula:  $\delta^{66}/^{64}\text{Zn} (\text{‰}) = (\delta^{66}/^{64}\text{Zn}_{\text{sample}}/\delta^{66}/^{64}\text{Zn}_{\text{IRMM 3702}} - 1) \times 1000$ . Repeated analyses of IRMM 3702 and NIST SRM 683 yielded an average  $\delta^{66}/^{64}\text{Zn}$  value of  $0.00 \pm 0.03\text{‰}$  ( $n = 56$ ) and  $-0.15 \pm 0.03\text{‰}$  ( $n = 6$ ), respectively, in agreement with the recommended  $\delta^{66}/^{64}\text{Zn}$  values for IRMM 3702 (0.00‰; Zhu et al., 2020) and NIST SRM 683 (-0.12‰; Yang et al., 2018). Since most of the Zn isotope values are published relative to the Johnson Matthey Zn "Lyon solution" (JMC Lyon Zn standard 3-0749L), the most widely accepted international Zn isotope standard. Thus, the Maoping sphalerite  $\delta^{66}\text{Zn}_{\text{JMC}}$  values were calculated with the equation:  $\delta^{66}\text{Zn}_{\text{JMC}} = \delta^{66}\text{Zn}_{\text{IRMM3702}} + 0.27$  (Table 2; Wang et al., 2017). For Cd isotopes, NIST SRM 3108 and JMC Cd (lot#74-075219 k) were used as the internal and secondary standard, respectively. The sample  $\delta^{114}/^{110}\text{Cd}$  values (relative to NIST SRM 3108) were calculated with the equation:  $\delta^{114}/^{110}\text{Cd} (\text{‰}) = (\delta^{114}/^{110}\text{Cd}_{\text{sample}}/\delta^{114}/^{110}\text{Cd}_{\text{NIST SRM 3108}} - 1) \times 1000$ . Average  $\delta^{114}/^{110}\text{Cd}$  values obtained from repeated analyses of NIST SRM 3108 ( $0.00 \pm 0.05\text{‰}$ ,  $n = 52$ ) and JMC Cd solution ( $-1.64 \pm 0.06\text{‰}$ ,  $n = 4$ ) are consistent with their respective recommended values, i.e., NIST SRM 3108 ( $\delta^{114}/^{110}\text{Cd} = 0.00\text{‰}$ ; Zhang et al., 2016) and JMC (-1.56 to -1.63‰; Zhang et al., 2016). All the Maoping sphalerite  $\delta^{114}/^{110}\text{Cd}$  values are given relative to the internal reference standard Spex Cd ( $\delta^{114}\text{Cd}_{\text{spex}} = \delta^{114}\text{Cd}_{\text{NIST SRM 3108}} + 0.11$ ; Zhang et al., 2016) (Table 2).

### 4. Results

#### 4.1. Lead isotope compositions

The sphalerite samples ( $n = 11$ ) from No. I-1 orebody have  $^{206}\text{Pb}/^{204}\text{Pb} = 18.725\text{--}18.751$ ,  $^{207}\text{Pb}/^{204}\text{Pb} = 15.764\text{--}15.768$ , and  $^{208}\text{Pb}/^{204}\text{Pb} = 39.381\text{--}39.436$ . Meanwhile, sphalerite samples ( $n = 15$ ) from No. I-2 orebody have  $^{206}\text{Pb}/^{204}\text{Pb} = 18.675\text{--}18.748$ ,  $^{207}\text{Pb}/^{204}\text{Pb} = 15.758\text{--}15.768$ , and  $^{208}\text{Pb}/^{204}\text{Pb} = 39.287\text{--}39.436$  (Table 1; Figs. 4 and 5).

**Table 2**

Zinc-cadmium contents and isotope compositions of sphalerite and potential metal source rocks for the Maoping deposit.

Sample	Object	Position	Oreboddy	$\delta^{66}\text{Zn}_{\text{JMC}}/\text{\textperthousand}$	2SD	$\delta^{114}\text{Cd}_{\text{spx}}/\text{\textperthousand}$	2SD	Zn/%	Cd/ppm	Cd/Zn	Source
MP-16-09	Brown-Yellow Sp	760 m	I-1	+0.12	0.02	–	–	50	2361	0.005	This paper
MP-16-14	Brown Sp	760 m	I-1	+0.13	0.02	–	–	51	2368	0.005	
MP-16-15	Brown-Yellow Sp	760 m	I-1	+0.23	0.04	+0.27	0.01	55	2535	0.005	
MP-16-16	Brown Sp	760 m	I-1	+0.14	0.03	+0.16	0.05	52	2885	0.006	
MP-16-17	Brown-Yellow Sp	760 m	I-1	+0.15	0.02	+0.07	0.06	47	2246	0.005	
MP-16-18	Brown-Yellow Sp	760 m	I-1	+0.08	0.00	+0.12	0.05	54	2950	0.006	
MP-16-22-1	Light-Yellow Sp	760 m	I-1	+0.25	0.00	+0.14	0.03	55	1869	0.003	
MP-16-22-2	Brown-Yellow Sp	760 m	I-1	+0.25	0.02	+0.09	0.01	51	1967	0.004	
MP-16-32	Brown-Yellow Sp	720 m	I-1	+0.18	0.01	+0.13	0.06	55	2623	0.005	
MP-16-37	Brown-Yellow Sp	720 m	I-1	+0.20	0.02	+0.02	0.03	50	2361	0.005	
MP-16-70	Brown-Yellow Sp	720 m	I-2	+0.11	0.03	+0.15	0.06	53	2525	0.005	
MP-16-72	Light-Yellow Sp	720 m	I-2	+0.20	0.06	+0.06	0.03	57	2557	0.004	
MP-16-73	Brown-Yellow Sp	720 m	I-2	+0.20	0.02	+0.15	0.07	51	1869	0.004	
MP-16-75	Brown Sp	720 m	I-2	+0.18	0.04	+0.03	0.01	53	2361	0.004	
MP-16-82	Brown-Yellow Sp	720 m	I-2	+0.23	0.01	-0.10	0.01	61	2623	0.004	
MP-16-86	Brown-Yellow Sp	720 m	I-2	+0.25	0.02	-0.05	0.06	53	2623	0.005	
MP-16-40	Light-Yellow Sp	670 m	I-2	+0.10	0.05	+0.12	0.01	53	2426	0.005	
MP-16-41	Brown-Yellow Sp	670 m	I-2	+0.11	0.03	+0.27	0.04	51	2262	0.004	
MP-16-45	Brown Sp	670 m	I-2	0.00	0.03	+0.22	0.09	49	3148	0.006	
MP-16-49	Brown-Yellow Sp	670 m	I-2	+0.23	0.04	+0.23	0.08	50	2230	0.004	
MP-16-58	Brown Sp	640 m	I-2	-0.05	0.05	+0.25	0.02	51	3148	0.006	
MP-16-61-1	Brown Sp	640 m	I-2	-0.07	0.02	+0.23	0.04	56	3344	0.006	
MP-16-61-2	Light-Yellow Sp	640 m	I-2	+0.11	0.02	+0.25	0.07	49	2459	0.005	
D09-3	Sedimentary rock	MDHF		-0.19 +0.06	0.06						Zhou et al., 2014a
D09-5	Limestone	UDZF		-0.22	0.05						
D09-7	Limestone	UDZF		+0.01	0.03						
TBS16-2	Graywacke	Basements: Kunyang & WC-1	Dolostone	+0.30	0.03						Zhu, 2014 He, 2017
Td1900-8	Dolostone	Huili Gp.		+0.21	0.04						
	Phyllite			+0.15	0.05						
Td1900-3	Phyllite			+0.34	0.02						
TBDB-4	Sandstone			+0.62	0.01						
TBS16-1	Graywacke			+0.33	0.05						
HS-8	Dolostone			+0.28	0.00						
YM-3	Breccia			+0.53	0.02						
EMS-1	Basalt			+0.35							
EMS-2	Basalt			+0.34							
EMS-3	Basalt			+0.29							
EMS-4	Basalt			+0.25							
EMS-5	Basalt			+0.27							
Ems09-14	Basalt			+0.32	0.06						
Ems09-15	Basalt			+0.30	0.04						
Ems09-16	Basalt			+0.44	0.10						

Abbreviations: MDHF-Middle Devonian Haikou Formation; UDZF-Upper Devonian Zaige Formation; Sp-Sphalerite

#### 4.2. Zinc isotope compositions

Sphalerite samples ( $n = 23$ ) from No. I orebody have homogeneous  $\delta^{66}\text{Zn}_{\text{JMC}}$  values of  $-0.07$  to  $+0.25\text{\textperthousand}$  (mean  $+0.14\text{\textperthousand}$ ; Fig. 6a). Sphalerite  $\delta^{66}\text{Zn}_{\text{JMC}}$  values of the upper and lower No. I-1 orebody are  $+0.08$  to  $+0.25\text{\textperthousand}$  (mean  $+0.17\text{\textperthousand}$ ,  $n = 10$ ) and  $-0.07$  to  $+0.25\text{\textperthousand}$  (mean  $+0.12\text{\textperthousand}$ ,  $n = 13$ ), respectively (Table 2).

#### 4.3. Cadmium isotope compositions

The same batch of sphalerite samples ( $n = 21$ ) have uniform  $\delta^{114}\text{Cd}_{\text{spx}}$  values ( $-0.10$  to  $+0.27\text{\textperthousand}$ , mean  $+0.13\text{\textperthousand}$ ; Fig. 6b) with Cd = 1869–3344 ppm (mean 2510 ppm,  $n = 23$ ). Sphalerite  $\delta^{114}\text{Cd}_{\text{spx}}$  values of the upper No. I-1 and lower No. I-2 orebodies are  $+0.02$  to  $+0.27\text{\textperthousand}$  (mean  $+0.13\text{\textperthousand}$ ,  $n = 8$ ) and  $-0.10$  to  $+0.27\text{\textperthousand}$  (mean  $+0.14\text{\textperthousand}$ ,  $n = 13$ ), respectively (Table 2).

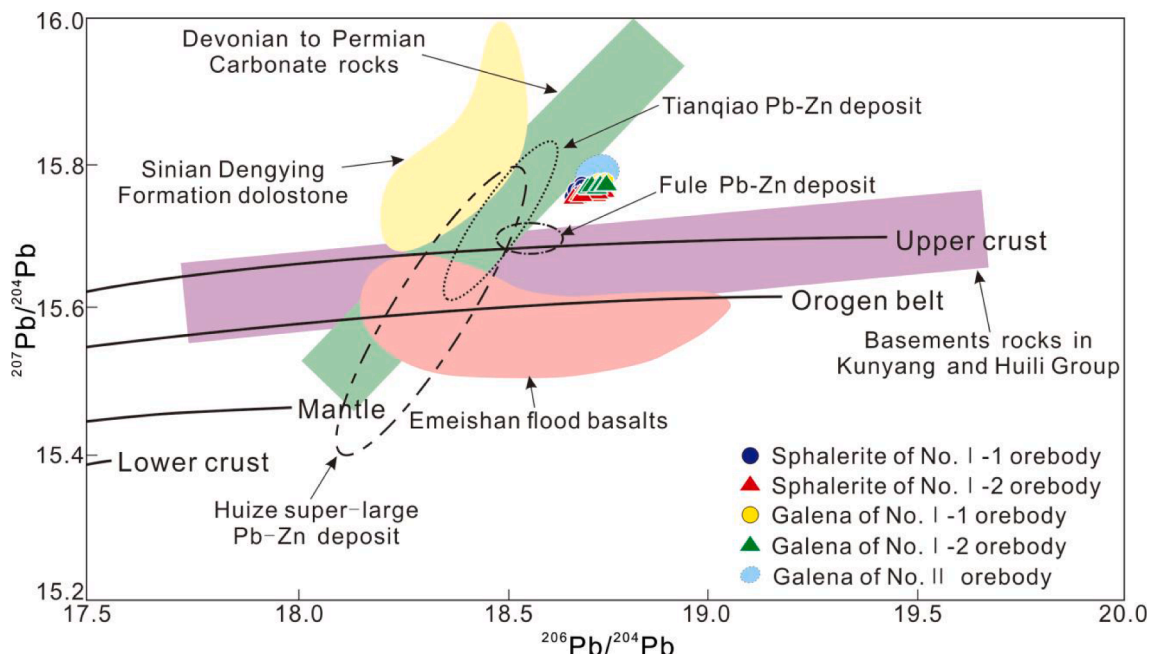


**Fig. 4.** Plots of  $^{207}\text{Pb}/^{204}\text{Pb}$  vs.  $^{206}\text{Pb}/^{204}\text{Pb}$  of sphalerites from the Maoping No. I orebody. Lead evolution curves are from Zartman and Doe (1981). Lead isotope data sources Devonian-Permian carbonates, Sinian Dengying Fm. dolostone, Kunyang/Huili Gp. basement, Emeishan flood basalts, and Huize deposit (Huang et al. 2004); Tianqiao deposit (Zhou et al., 2013); Fule deposit (Zhou et al., 2018b); Galena from Maoping deposit: No. I orebody (He et al., 2020) and No. II orebody (Tan et al., 2019; Xiang et al., 2020).

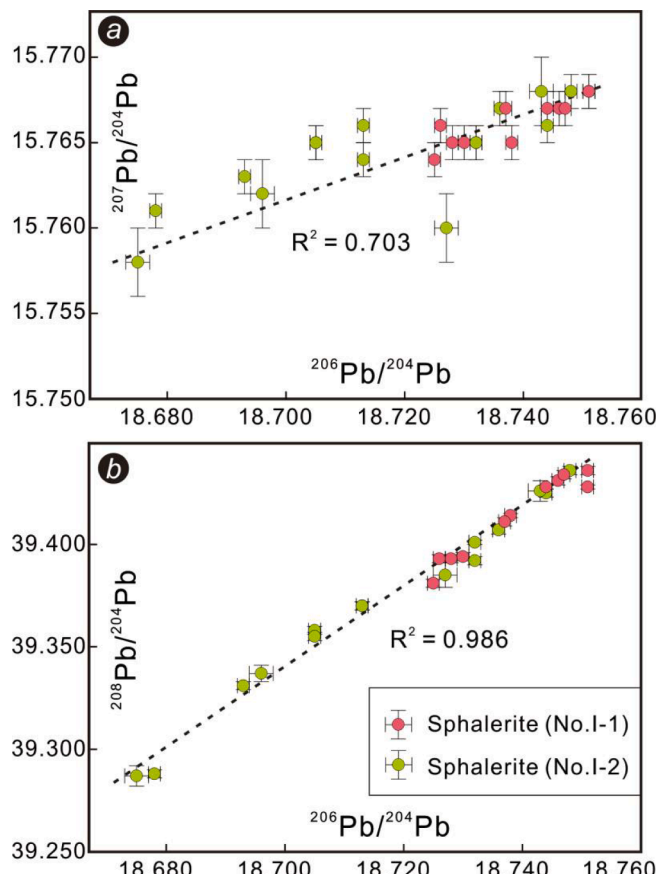


**Fig. 5.** Plots of  $^{207}\text{Pb}/^{204}\text{Pb}$  vs.  $^{206}\text{Pb}/^{204}\text{Pb}$  (a) and  $^{208}\text{Pb}/^{204}\text{Pb}$  vs.  $^{206}\text{Pb}/^{204}\text{Pb}$  (b) of sphalerites and galenas from the Maoping No. I orebody. Galena Pb isotope data are from He et al. (2020).

## 5. Discussion

### 5.1. Source of lead at Maoping

As shown in Fig. 4, the Maoping sphalerite samples have narrow ranges of Pb isotope ratios ( $^{206}\text{Pb}/^{204}\text{Pb} = 18.68\text{--}18.75$ ,  $^{207}\text{Pb}/^{204}\text{Pb} = 15.76\text{--}15.77$ ,  $^{208}\text{Pb}/^{204}\text{Pb} = 38.29\text{--}38.44$ ; Table 1), similar to the galena samples from Nos. I-II orebodies ( $^{206}\text{Pb}/^{204}\text{Pb} = 18.71\text{--}18.77$ ,  $^{207}\text{Pb}/^{204}\text{Pb} = 15.77\text{--}15.80$ ,  $^{208}\text{Pb}/^{204}\text{Pb} = 39.38\text{--}39.53$ ; Tan et al., 2019; He et al., 2020; Xiang et al., 2020). This suggests that the lead in galena and sphalerite was probably derived from the same source.

At Maoping, Pb isotope data of all sulfide samples plot well above the average upper crustal Pb evolution line in the  $^{207}\text{Pb}/^{204}\text{Pb}$  vs.  $^{206}\text{Pb}/^{204}\text{Pb}$  diagram (Fig. 4), suggesting a homogeneous or mixed source derived from the upper crust (Zartman and Doe, 1981; Carr et al., 1995; Zhou et al., 2018b; Wu et al., 2020). Previous studies suggested three potential upper-crustal lead sources in the SYGMP, i.e., (1) the Neoproterozoic Kunyang/Huili Gp. basement rocks, (2) Late Permian Emeishan basalts, and (3) the Sinian to Permian carbonate ore host (Liu and Lin, 1999; Huang et al., 2004; Zhou et al., 2013a, 2018a). Nevertheless, the Pb isotope compositions of the Maoping sulfides are very different from each of the age-corrected (202.5 Ma; Yang et al., 2019) potential source rocks above-mentioned (Fig. 4), precluding a single lead source.

It is likely that the ore lead at Maoping could be originated from the mixing of two isotopically distinct sources (high- $\mu$  and low- $\mu$  source, where  $\mu = \text{Th}/\text{U}$ ), as supported by the positive linear correlations of  $^{207}\text{Pb}/^{204}\text{Pb}$  vs.  $^{206}\text{Pb}/^{204}\text{Pb}$  ( $r^2 = 0.703$ ; Fig. 5a) and  $^{208}\text{Pb}/^{204}\text{Pb}$  vs.  $^{206}\text{Pb}/^{204}\text{Pb}$  ( $r^2 = 0.986$ ; Fig. 5b). The Pb isotope compositions are plotted near the age-corrected Devonian to Permian carbonate rocks (Fig. 4). Carbonate rocks are U-enriched but Th-depleted (Ostendorf et al., 2017; Rosa et al., 2016), which can account for the low- $\mu$  source. The basement rocks and Late Permian Emeishan basalts are characterized by high  $\mu$ , and can therefore represent the high- $\mu$  end-member source (Dostal and Capedri, 1978; Downes et al., 2001). A major lead input from the Emeishan basalt could be ruled out for the following

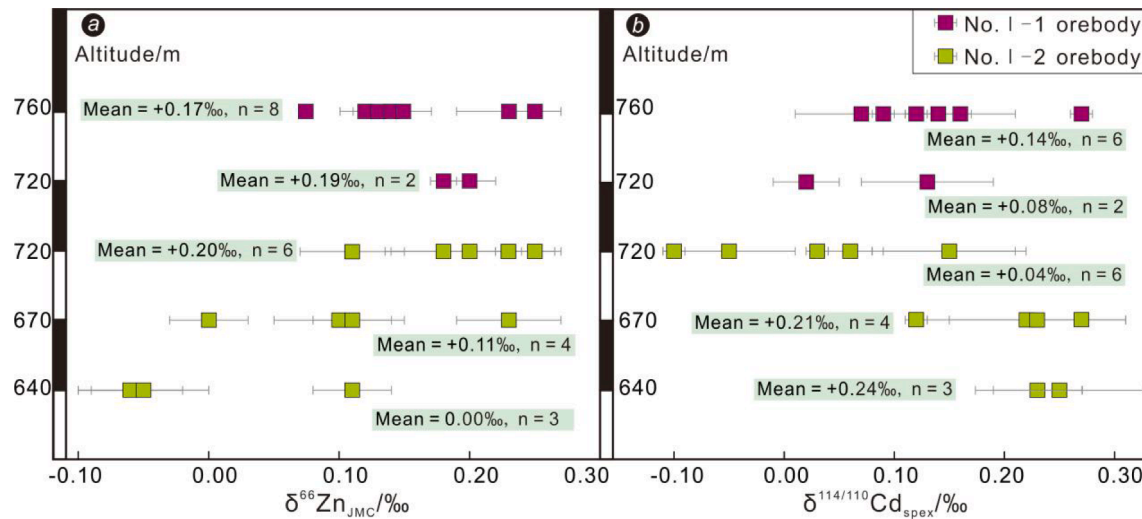


Fig. 6.  $\delta^{66}\text{Zn}_{\text{JMC}}$  (a) and  $\delta^{114}\text{Cd}_{\text{spex}}$  (b) isotope values of sphalerites from the Maoping No. I orebody.

reasons: (1) the basalt contains higher Cu (6–323 µg/g) and Ni (16–1160 µg/g) contents than Pb (66–156 µg/g) and Zn (6–30 µg/g) (Xu et al., 2001; Huang et al., 2004). If it contributed significant amounts of metals for the mineralization, abundant Cu-Ni sulfide minerals would also be expected, which were not observed or reported at Maoping (Wei et al., 2015, 2021; Xiang et al., 2020; He et al., 2020); (2) leaching experiments show that Pb and Zn are difficult to be extracted from basalt by hydrothermal fluid (Li et al., 2012).

It is noteworthy that sphalerite grains from the upper No. I-1 orebody are slightly enriched in radiogenic Pb than those from the lower No. I-2 orebody (Fig. 5). This could be interpreted by different proportions of source mixing between the basement rocks and carbonate wallrocks, in which the wallrock lead input decreased with depths. Overall, we consider that the Devonian-Carboniferous carbonate wallrocks provided the majority of the ore lead, with a significant basement rock contribution especially at depth, in agreement with the in-situ galena Pb

isotope data (Xiang et al., 2020). A similar conclusion was yielded in the nearby Yunluheba deposit (Tang et al., 2019).

## 5.2. Zinc-cadmium isotope variation and ore-fluid mixing

Zn and Cd have similar geochemical behavior and crystallographic properties, with the latter usually occurring as isomorph (0.2–3.0 wt%) in sphalerite (Schwartz, 2000; Yang et al., 2015; Zhu et al., 2016). Previous studies suggested that the Zn and Cd isotope fractionation is also largely similar in low-medium temperature hydrothermal systems (Wen et al., 2016; Xu et al., 2019). There are three possible causes for the Zn-Cd isotope variation in sphalerite precipitation, i.e., (1) fluctuation of ore-fluid temperature (Maréchal and Sheppard, 2002; John et al., 2008), (2) kinetic Raleigh fractionation between hydrothermal fluid and sphalerite (Kelley et al., 2009; Gagnevin et al., 2012; Zhou et al., 2014a), and (3) mixing of fluid sources with different Zn isotope compositions

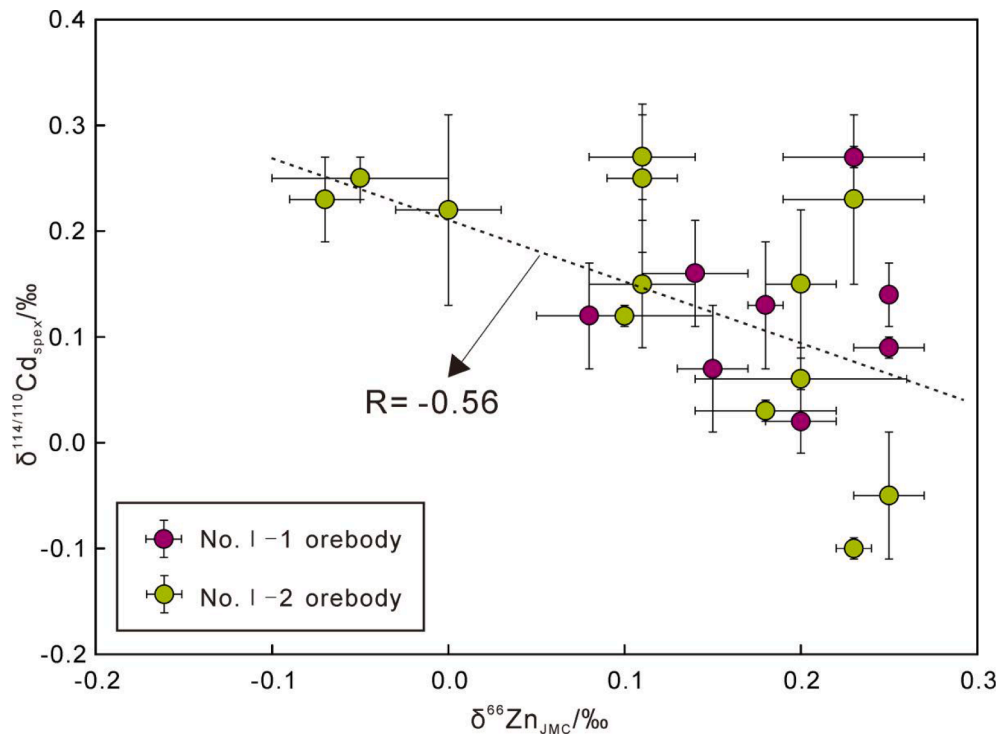
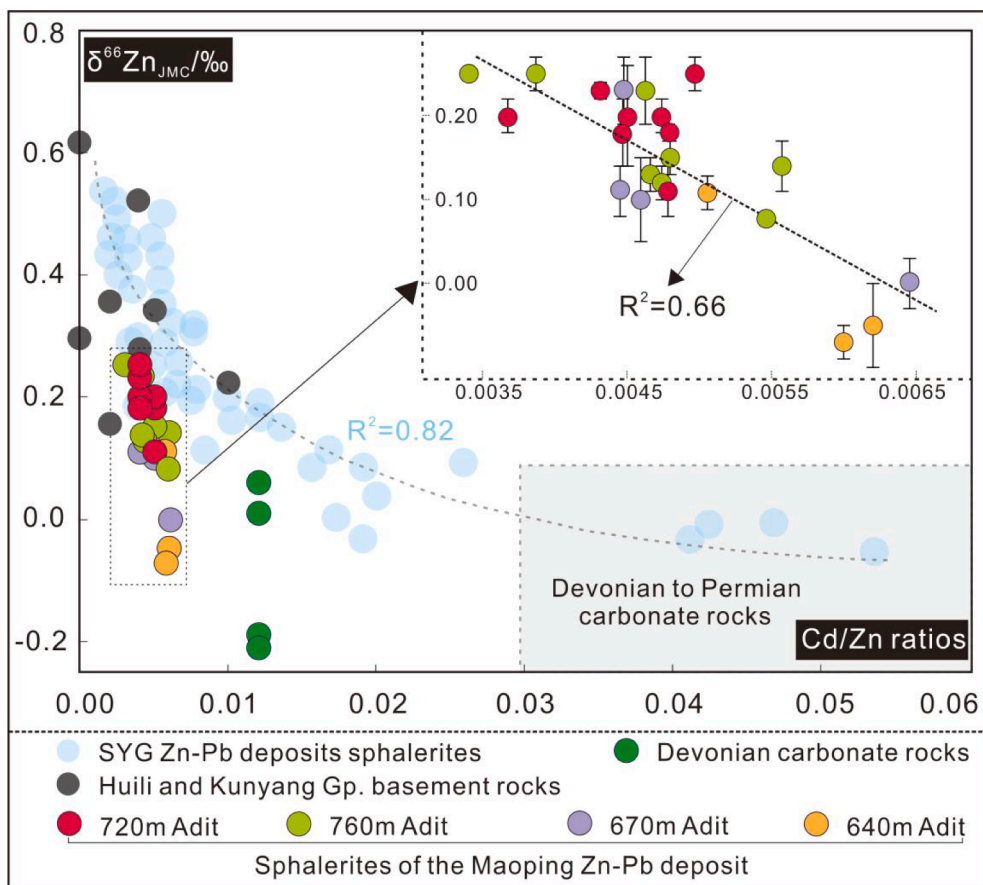


Fig. 7.  $\delta^{114}\text{Cd}_{\text{spex}}$  vs.  $\delta^{66}\text{Zn}_{\text{JMC}}$  plot of sphalerites from Maoping No. I orebody.



**Fig. 8.** Sphalerite  $\delta^{66}\text{Zn}_{\text{JMC}}$  vs. Cd/Zn plot for the Maoping deposit, Huili/Kunyang Gp. basement rocks (He, 2017), and Devonian ore-hosting carbonate wallrocks (Zhu, 2014; Zhou et al., 2014a). Data of the SYG ore sphalerites are from Zhu et al. (2020).

(Wilkinson et al., 2005; He et al., 2016; Zhang et al., 2019b; Zhu et al., 2020).

At Maoping, the homogenization temperatures of sphalerite fluid inclusions fall within a narrow range (180 to 218 °C, Han et al., 2007). It was suggested that temperature change may have caused the sphalerite  $\delta^{66}\text{Zn}_{\text{JMC}}$  (−0.07 to + 0.25‰) and  $\delta^{114}\text{Cd}_{\text{spex}}$  (−0.10 to + 0.27‰) variations. However, it is found that no  $\delta^{66}\text{Zn}_{\text{JMC}}$  vs. temperature correlation exists at < 300 °C, as supported by both experimental (30–50 °C; Maréchal and Sheppard, 2002) and hydrothermal ore deposit (60–240 °C; Wilkinson et al., 2005) studies. This conclusion is further supported by that the published sphalerite  $\delta^{66}\text{Zn}_{\text{JMC}}$  values (−0.26 to + 0.71‰) from many SYG Pb-Zn deposits (e.g., Dalianzhi, Maozu, Wusihe, Tianbaoshan, and Tianqiao) have no correlation with their respective fluid inclusion homogenization temperature (120–280 °C) (Zhou et al., 2014a, 2018b; Zhang et al., 2019a; Xu et al., 2019; Zhu et al., 2020). Therefore, the ore-forming temperature has likely little influence on the Zn-Cd isotope variation.

Experimental studies and theoretical calculations demonstrated that the early precipitated sulfides have lower Cd content and  $\delta^{66}\text{Zn}$  and  $\delta^{114}\text{Cd}$  values than those of the late precipitated sulfides (Archer et al., 2004; Fujii et al., 2011; Yang et al., 2015). Some other studies confirmed that Rayleigh distillation could fractionate Zn isotopes between sphalerite and ore fluid, resulting in systematically increasing sphalerite  $\delta^{66}\text{Zn}$  and  $\delta^{114}\text{Cd}$  values toward the late hydrothermal stages (Wilkinson et al., 2005; Kelley et al., 2009; Gagnepain et al., 2012; Zhou et al., 2014a; Zhu et al., 2016; Gao et al., 2017). If the Zn-Cd isotope variation was mainly controlled by Rayleigh fractionation, the  $\delta^{66}\text{Zn}$  and  $\delta^{114}\text{Cd}$  values would increase gradually from the early (brown) to late (brownish-yellow and light-yellow) Maoping sphalerite. However,

$\delta^{66}\text{Zn}$  value of the early brown sphalerite (−0.07 to + 0.18‰, avg. + 0.06‰) are lower than those of the late brownish-yellow/light-yellow sphalerite (+0.08 to + 0.25‰, avg. + 0.18‰) (Table 2), whereas the  $\delta^{114}\text{Cd}$  values of the early sphalerite (+0.03 to + 0.25‰, avg. + 0.19‰) are higher than those of the late sphalerite (−0.10 to + 0.27‰, avg. + 0.12‰) (Table 2). Hence, Raleigh fractionation alone could not account for the observed Zn-Cd isotope variation here, as supported by the negative correlations in  $\delta^{66}\text{Zn}_{\text{JMC}}$  vs.  $\delta^{114}\text{Cd}_{\text{spex}}$  (Fig. 7) and  $\delta^{66}\text{Zn}_{\text{JMC}}$  vs. Cd/Zn (Fig. 8).

Thus, isotope evidence suggests that ore-fluid mixing between different isotope end-members may occur during the Maoping Pb-Zn mineralization. A fluid-mixing metallogenetic model was proposed for many Pb-Zn deposits in the SYG region (Huang et al., 2004; He et al., 2016; Luo et al., 2019; Zhang et al., 2019b; Wei et al., 2021). Zhu et al. (2020) proposed a binary fluid-mixing model based on the logarithmic regression of sphalerite  $\delta^{66}\text{Zn}_{\text{JMC}}$  vs. Cd/Zn for the SYG Ediacaran Dengying Formation-hosted Pb-Zn deposits (Fig. 8). In the  $\delta^{66}\text{Zn}_{\text{JMC}}$  vs. Cd/Zn plot (Fig. 8), the Maoping sphalerite samples fall along a steep linear trend ( $r^2 = 0.66$ ) between the basement rocks and carbonate wallrocks, suggesting that the narrow sphalerite Zn-Cd isotopic ranges can be ascribed to binary fluid mixing, including a high  $\delta^{66}\text{Zn}$ -low Cd/Zn end-member and a low  $\delta^{66}\text{Zn}$ -high Cd/Zn end-member (Fig. 8).

### 5.3. Source of zinc at Maoping

As above-mentioned, the narrow sphalerite  $\delta^{66}\text{Zn}$  range at Maoping is mainly due to ore-fluid mixing, and thus the sphalerite Zn isotopes should approximate those of the ore fluids. Previous studies have proposed the Neoproterozoic basement rocks, Emeishan flood basalts, and/

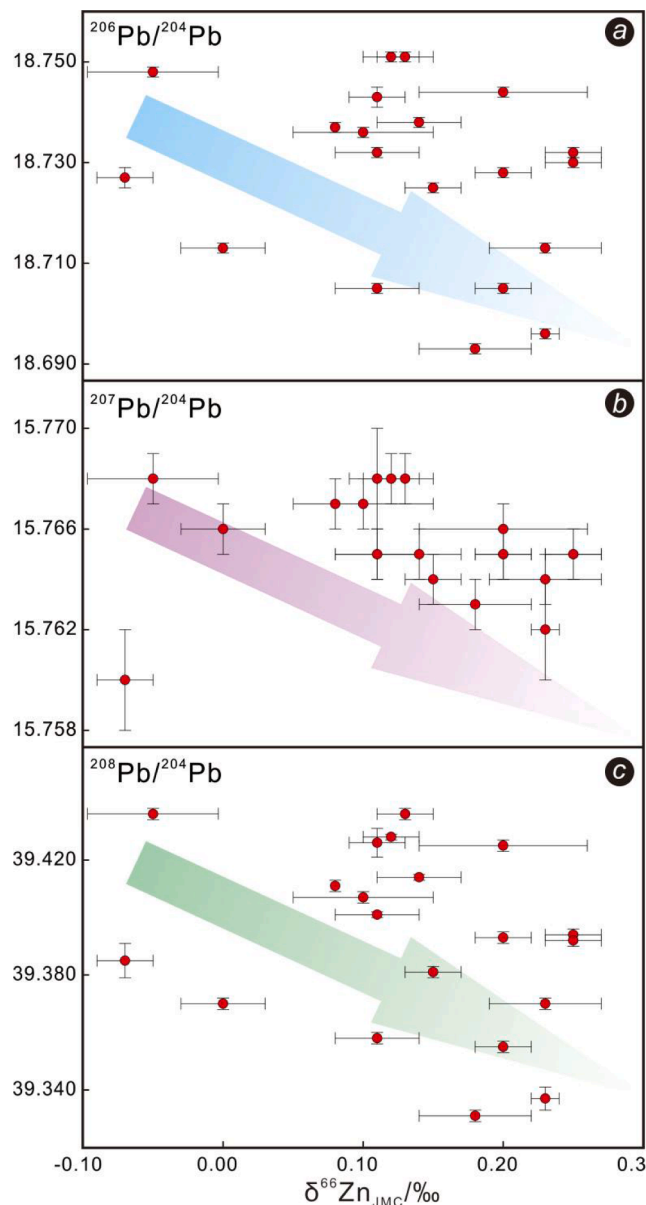


**Fig. 9.** Plots of  $^{206}\text{Pb}/^{204}\text{Pb}$  (a),  $^{207}\text{Pb}/^{204}\text{Pb}$  (b), and  $^{208}\text{Pb}/^{204}\text{Pb}$  (c) versus  $\delta^{66}\text{Zn}_{\text{JMC}}$  of sphalerites from the Maoping No. I orebody.

or carbonate wallrocks to be potential ore zinc source in the SYGMP (Liu and Lin, 1999; Huang et al., 2004; Zhou et al., 2013a). The basalt  $\delta^{66}\text{Zn}_{\text{JMC}}$  values (+0.25 to + 0.44‰, avg. + 0.32‰; Fig. 10; Wu, 2013; Zhou et al., 2014a) are generally higher than that of the Maoping sphalerite (−0.07 to + 0.25‰, avg. + 0.14‰; Table 2). If the Emeishan basalts were a major Zn source, the  $\delta^{66}\text{Zn}$  would increase with decreasing distance from the Pb-Zn orebody and the basalt. However, the sphalerite  $\delta^{66}\text{Zn}$  values are roughly similar from 640 to 760 m depth at Maoping. Meanwhile,  $\delta^{66}\text{Zn}$  values of the Fule deposit in the SYGMP (0.09 to + 0.33‰; Xu et al., 2019) that is also spatially (~1 m) close to the Emeishan basalts are far lower than those of the overlying Sinian carbonate-hosted Tanbaoshan deposit (0.18 to + 0.73‰; He et al., 2016). This suggests that the Emeishan basalt could not be a major source of the ore zinc.

The Maoping sphalerite  $\delta^{66}\text{Zn}_{\text{JMC}}$  data (−0.07 to + 0.25‰) fall between the fields of the Devonian carbonate wallrocks (−0.22 to + 0.06‰; Fig. 10; Zhou et al., 2014a, 2014b; Zhu, 2014) and the Neoproterozoic basement rocks (+0.15 to + 0.62‰; Fig. 10; He, 2017), and the mean

(+0.14‰) is closer to the basement rocks (Fig. 8). This indicates that both rock types may have contributed different proportions of zinc and lead to the Maoping deposit. The negative linear correlation between sphalerite  $\delta^{66}\text{Zn}_{\text{JMC}}$  and Pb isotope ratios (Fig. 9a–c) also indicates that the ore lead and zinc at Maoping may have sourced from two different end-members, namely the basement-derived fluid with heavier Zn but lighter Pb isotopes, and the carbonate-derived fluid with lighter Zn but heavier Pb isotopes.

#### 5.4. Implication for Maoping Pb-Zn mineralization

The genesis of the Maoping Pb-Zn deposit is mainly disputable on sedimentary-reworking (Liu and Lin, 1999), hydrothermal modified SEDEX (Wang et al. 2009), and MVT (He et al., 2020; Wei et al., 2021). The epigenetic hydrothermal mineralization features (ore-controlling fault and fold, Figs. 1 and 2; lenticular and veined orebodies, Fig. 2; ore fabrics, Fig. 3) and the multilayered Pb-Zn metallogenesis in carbonate rocks rather than the clastic rocks (the ore-host of SEDEX) suggest that the Maoping deposit could not be a *syn*-sedimentary or SEDEX origin. The similar geological and geochemical characteristics between Pb-Zn deposits in the SYGMP (e.g., Maoping, Huize, Fule, Daliangzi, Maozu) and typical MVT Pb-Zn deposits around the world (Table 3; Fig. 10) indicate that the Maoping deposit is best classified as MVT. This is also supported by the evidence that all sphalerite samples from Maoping have  $\delta^{114}\text{Cd}_{\text{spex}}$  values (−0.10 to + 0.27‰) and  $1/\text{Cd}$  ratios ( $0.3 \times 10^{-3}$  to  $0.5 \times 10^{-3}$ ) falling into the MVT field (Fig. 11; Zhu et al., 2013, 2018; Xu et al., 2019).

MVT Pb-Zn mineralization is closely related to the large compressive events caused by regional orogenic activity (Leach and Rowan, 1986; Leach et al., 2001, 2010). Sphalerite Rb-Sr dating (202.5 Ma; Yang et al., 2019) indicates that the Devonian-Carboniferous carbonate-hosted Pb-Zn mineralization at Maoping occurred in the Early Jurassic, during which late Indosinian orogenic activities were active in the SYGMP (Cai and Zhang, 2009; Hu et al., 2017; Zhou et al., 2018a). At Maoping, the basement-derived Zn-bearing hydrothermal fluid was likely driven by regional compression and migrated along the regional Xiaojiang fault and associated fractures (Fig. 1b) to the porous Devonian-Carboniferous carbonate rocks. During the migration, abundant ore-forming materials (mainly lead) were leached from the carbonate wallrocks by the hydrothermal fluids. Subsequently, this metal-bearing fluid was trapped by the local Shimenkan anticline and its associated NE-trending interlayer faults (Fig. 2a-b). The interconnected open-space structure formed by faults and folds allowed the mixing of metal-bearing fluids with reduced S-bearing fluids, from which the reduced sulfur was generated by the TSR of the Devonian-Carboniferous marine sulfates (Ren et al., 2018; He et al., 2020). The fluid mixing may have resulted in the sulfide precipitation and increase the fluid acidity  $[(\text{Fe}, \text{Zn}, \text{Pb})\text{Cl}(\text{aq}) + \text{H}_2\text{S}(\text{aq}) = (\text{Fe}, \text{Zn}, \text{Pb})\text{S}(\text{s}) + \text{H}^+ + 4\text{Cl}^-]$ ; Anderson, 2008]. Further interaction between this acidic ore-forming fluid and carbonate wallrocks increase the porosity for high-grade sulfide ore precipitation at Maoping.

#### 6. Conclusions

- 1 Sphalerite Pb isotope compositions indicate that the ore lead was mainly derived from the Devonian-Carboniferous carbonate wallrocks with significant contributions from the Neoproterozoic basement rocks.
- 2 The similar sphalerite Zn-Cd isotope compositions may be attributed mainly to the binary source mixing between the metamorphic basement (major) and the ore-bearing carbonate sequence (minor).
- 3 Deposit geological features and sulfide trace element and Pb-Zn-Cd isotope evidence altogether suggest that the Maoping Pb-Zn deposit is best classified as Mississippi Valley-type. The Zn-rich basement-derived hydrothermal fluid may have ascended along the regional fault and its secondary structures, circulated and extracted ore-forming materials from various wallrock sequences. The metal-rich

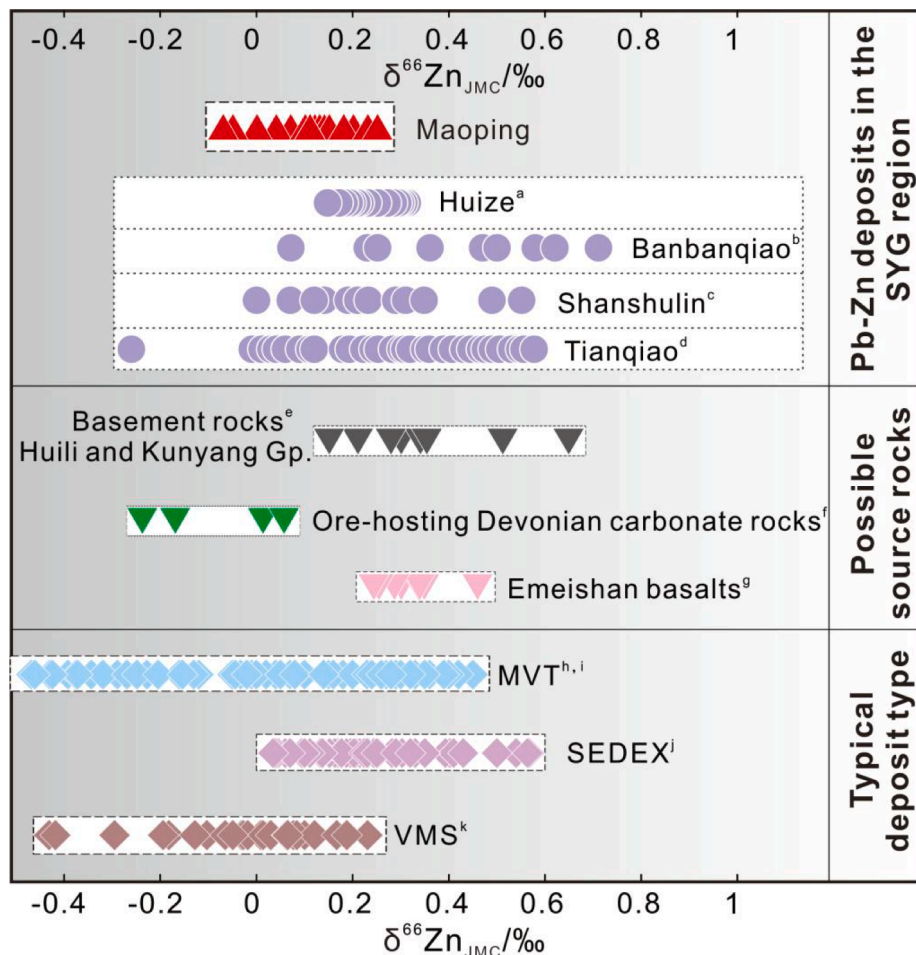


**Fig. 10.**  $\delta^{66}\text{Zn}_{\text{JMC}}$  distribution diagram for major Pb-Zn deposits and possible source rocks in the SYG region, together with typical Pb-Zn deposit types. Data source: <sup>a</sup>Wu, 2013; <sup>b,d</sup>Zhou et al., 2014a; <sup>c</sup>Zhou et al., 2014b; <sup>e</sup>He, 2017; <sup>f</sup>Zhu, 2014, Zhou et al., 2014a; <sup>g</sup>Wu, 2013, Zhou et al., 2014a; <sup>h</sup>Albarède (2004); <sup>i</sup>Pašava et al., 2014; <sup>j</sup>Kelley et al., 2009; <sup>k</sup>Mason et al., 2005.

**Table 3**

Geological comparison between the Maoping deposit, SYG Pb-Zn deposits, and Mississippi Valley-type (MVT) deposits.

Features	Maoping Pb-Zn deposit	MVT Pb-Zn deposit	SYG Pb-Zn deposits
Mineralization age	Epigenetic, Late Triassic (~202.5 Ma)	Epigenetic, Proterozoic to Cretaceous	Epigenetic, Late Triassic (200 ~ 225 Ma)
Tectonic setting	Carbonate platform	Carbonate platform, Foreland basin of passive continental margin	Carbonate platform (margin)
Host rocks	Dolostone and limestone	Carbonate rocks	Ediacaran to Permian carbonate rocks
Ore-controlling structures	Shimenkan anticline and Maoping fault	Faults, folds and lithology	Fault and anticline
Orebodies occurrences	Stratoid, lenticular and veined	Layered, stratoid, veined and lenticular	Stratoid, lenticular and veined
Ore structures	Massive, disseminated, veined and brecciated	Disseminated, massive, veined and brecciated	Massive, disseminated, veined and brecciated
Ore minerals	Sphalerite, galena, pyrite	Sphalerite, galena, pyrite and marcasite	Sphalerite, galena, pyrite
Gangue minerals	Dolomite and calcite	Dolomite, calcite, barite, fluorite, quartz and bitumen	Dolomite, calcite, quartz, barite, bitumen and fluorite
Ore-forming fluid	180–218°C, 4.1–9.5 wt% NaCl equiv.	50–250°C, 10–30 wt% NaCl equiv.	120–280°C, 10–30 wt% NaCl equiv.
Sphalerite trace elements	High Cd, Ge and low Mn, Fe, Co, Sn	High Cd, Ge, Ga and low Fe, Mn, In, Sn	High Cd, Ga, Ge and low Fe, Mn, In
Sulfur source(s)	TSR of marine sulfate in ore-hosting strata (sulfide $\delta^{34}\text{S}$ : +8.6 to + 25.7‰)	Seawater sulfate ( $\delta^{34}\text{S}$ : +10 to + 35‰)	TSR of marine sulfate in ore-hosting strata (sulfide $\delta^{34}\text{S}$ : -5.0 to + 30.0‰)
Metal source(s)	Devonian to Carboniferous ore-bearing rocks + Neoproterozoic basement rocks	Basement/ore-host/underlying strata	Neoproterozoic basement rocks + ore-bearing rocks + underlying strata
References	Han et al. (2007); Wei et al. (2012); Xiang et al. (2020); Wei et al. (2020); This study	Leach et al. (2005, 2010)	Huang et al. (2004); Zhou et al. (2013a, 2018a)

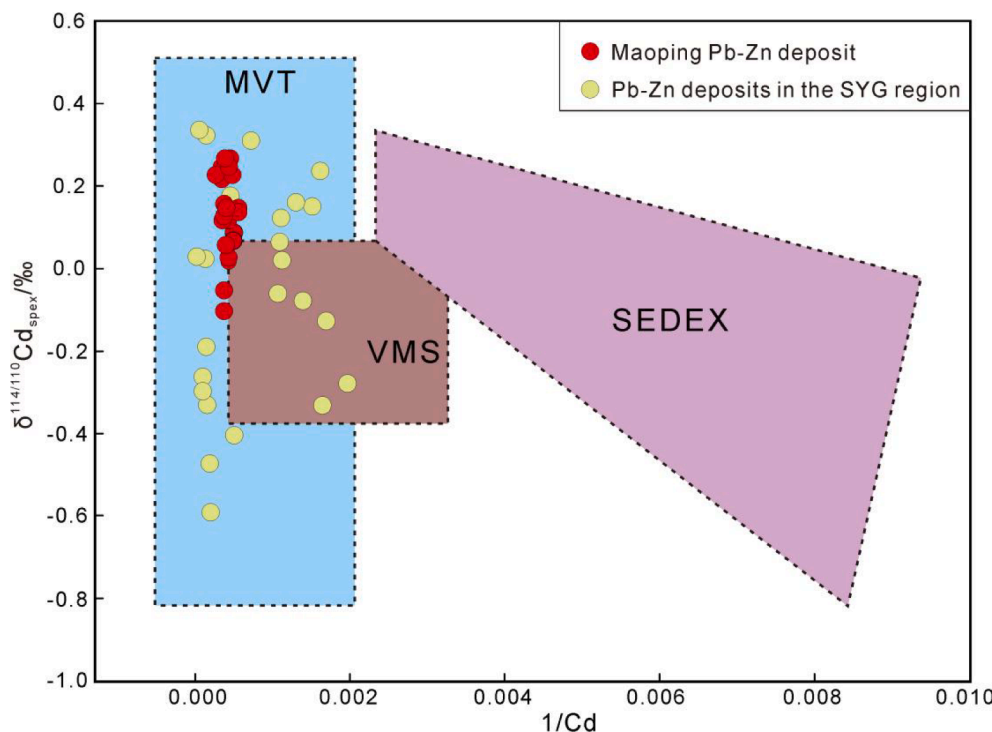


**Fig. 11.**  $\delta^{114}\text{Cd}_{\text{spex}}$  vs.  $1/\text{Cd}$  plot to discriminate different types of Pb-Zn deposits (modified after Zhu et al., 2013; Xu et al., 2019).

fluids may have then mixed with reduced S-bearing fluid trapped in the ore-hosting carbonate sequence and precipitated the sulfide ores.

#### Declaration of Competing Interest

The authors declare that they have no known competing financial interests or personal relationships that could have appeared to influence the work reported in this paper.

#### Acknowledgments

This study was supported by the National Natural Science Foundation of China (U1812402 and 41673056) and the Guizhou Provincial Science and Technology Planning Project ([2021]213). We are grateful to the Yiliang Chihong Mining Co. Ltd. for granting mine access and sampling. We are also indebted to the Editor-in-Chief Prof. Huayong Chen, and two anonymous reviewers for their insightful comments.

#### References

- Albarède, F., 2004. The stable isotope geochemistry of copper and zinc. *Rev. Mineral. Geochem.* 55, 409–427.
- Anderson, G.M., 2008. The mixing hypothesis and the origin of Mississippi Valley-Type ore deposits. *Econ. Geol.* 103, 1683–1690.
- Archer, C., Vance, D., Butler, I., 2004. Abiotic Zn isotope fractionations associated with ZnS precipitation. *Geochim. Cosmochim. Acta* 68, A325.
- Cai, J.X., Zhang, K.J., 2009. A new model for the Indochina and South China collision during the Late Permian to the Middle Triassic. *Tectonophysics* 467, 35–43.
- Carr, G.R., Dean, J.A., Suppel, D.W., Heithersay, P.S., 1995. Precise lead isotope fingerprinting of hydrothermal activity associated with Ordovician to Carboniferous metallogenic events in the Lachlan fold belt of New South Wales. *Econ. Geol.* 90, 1467–1505.
- Dostal, J., Capedri, S., 1978. Uranium in metamorphic rocks. *Contrib. Mineral. Petrol.* 66, 409–414.
- Downes, H., Markwick, A.J.W., Kempton, P.D., Thirlwall, M.F., 2001. The lower crust beneath cratonic north-east Europe: isotopic constraints from garnet granulite xenoliths. *Terra Nova* 13, 395–400.
- Fujii, T., Moynier, F., Pons, M.L., Albarède, F., 2011. The origin of Zn isotope fractionation in sulfides. *Geochim. Cosmochim. Acta* 75, 7632–7643.
- Gagnevin, D., Boyce, A.J., Barrie, C.D., Menuge, J.F., Blakeman, R.J., 2012. Zn, Fe and S isotope fractionation in a large hydrothermal system. *Geochim. Cosmochim. Acta* 88, 183–198.
- Gao, S., Yang, J., Zhou, L., Li, M., Hu, Z.C., Guo, J.L., Yuan, H.L., Gong, H.J., Xiao, G.Q., Wei, J.Q., 2011. Age and growth of the Archean Kongling terrain, South China, with emphasis on 3.3 Ga granitoids gneisses. *Am. J. Sci.* 311, 153–182.
- Gao, Z.F., Zhu, X.K., Sun, J., Luo, Z.H., Bao, C., Tang, C., Ma, J.X., 2017. Spatial evolution of Zn-Fe-Pb isotopes of sphalerite within a single ore body: A case study from the Dongshengmiao ore deposit, Inner Mongolia, China. *Miner. Depos.* 15, 1–11.
- Han, R.S., Zou, H.J., Hu, B., Hu, Y.Z., Xue, C.D., 2007. Features of fluid inclusions and sources of ore-forming fluid in the Maoping carbonate-hosted Zn-Pb-(Ag-Ge) deposit, Yunnan, China. *Acta Petrol. Sin.* 23, 2109–2118 (in Chinese with English abstract).
- He, C.Z., Xiao, C.Y., Wen, H.J., Zhou, T., Zhu, C.W., Fan, H.F., 2016. Zn-S isotopic compositions of the Tianbaoshan carbonate-hosted Zn-Pb deposit in Sichuan, China: Implications for source of ore components. *Acta Petrol. Sin.* 32, 3394–3406 (In Chinese with English abstract).
- He, C.Z., 2017. Zinc-Sulfur isotopic compositions of the Tianbaoshan carbonate-hosted Pb-Zn deposit in Sichuan, China: implications for source of ore components. Master dissertation, Institute of Geochemistry, Chinese Academy of Sciences, Guiyang, pp. 1–65 (in Chinese with English abstract).
- He, Y.F., Wu, T., Huang, Z.L., Ye, L., Deng, P., Xiang, Z.Z., 2020. Genesis of the Maoping carbonate-hosted Pb-Zn deposit, northeastern Yunnan Province, China: Evidences from geology and C-O-S-Pb isotopes. *Acta Geochim.* 39, 782–796.
- Hu, R.Z., Zhou, M.F., 2012. Multiple Mesozoic mineralization events in South China – An introduction to the thematic issue. *Miner. Depos.* 47, 579–588.
- Hu, R.Z., Fu, S.L., Huang, Y.H., Zhou, M.F., Fu, S.H., Zhao, C.H., Wang, Y.J., Bi, X.W., Xiao, J.F., 2017. The giant South China Mesozoic low-temperature metallogenic domain: Reviews and a new geodynamic model. *J. Asian Earth Sci.* 137, 9–34.
- Huang, Z.L., Chen, J., Han, R.S., Li, W.B., Liu, C.Q., Zhang, Z.L., Ma, D.Y., Gao, D.R., Yang, H.L., 2004. Geochemistry and ore genesis of the Huize Giant Pb-Zn deposit in Yunnan Province, China: discussion on the relationship between the Emeishan flood basalts and Pb-Zn mineralization. Geological Publishing House, Beijing, pp. 1–214 (in Chinese).
- Huang, Z.L., Hu, R.Z., Su, W.C., Wen, H.J., Liu, S., Fu, Y.Z., 2011. A study on the large-scale low-temperature metallogenic domain in southwestern China—Significance, History and New Progress. *Acta Mineralogica Sinica* 31, 309–314 (in Chinese with English abstract).
- John, S.G., Rouxel, O.J., Craddock, P.R., Engwall, A.M., Boyle, E.A., 2008. Zinc stable isotopes in seafloor hydrothermal vent fluids and chimneys. *Earth Planet. Sci. Lett.* 269, 17–28.
- Kelley, K.D., Wilkinson, J.J., Chapman, J.B., Crowther, H.L., Weiss, D.J., 2009. Zinc isotopes in sphalerite from base metal deposits in the Red Dog district, Northern Alaska. *Econ. Geol.* 104, 767–773.
- Leach, D.L., Rowan, E.L., 1986. Genetic link between Ouachita foldbelt tectonism and the Mississippi Valley-type lead-zinc deposits of the Ozarks. *Geology* 14, 931–935.

- Leach, D.L., Bradley, D.C., Lewchuk, M., Symons, D., Marsily, G., Brannon, J., 2001. Mississippi Valley-type lead-zinc deposits through geological time: Implications from recent age-dating research. *Miner. Depos.* 2001 (36), 711–740.
- Leach, D.L., Sangster, D.F., Kelley, K.D., Large, R.R., Garven, G., Allen, C.R., Gutzmer, J., Walters, S., 2005. Sediment-hosted lead-zinc deposits: A global perspective. *Econ. Geol.* 100, 561–607.
- Leach, D.L., Bradley, D.C., Huston, D., Pisarevsky, S.A., Taylor, R.D., Gardoll, S.J., 2010. Sediment-hosted lead-zinc deposits in earth history. *Econ. Geol.* 105, 593–625.
- Li, B., Gu, X.C., Wen, S.M., Han, R.S., Sheng, R., Xu, G.R., Cao, Y., Wu, H., Zou, G.F., 2012. Effect of Emeishan basalt in northeast Yunnan on lead and zinc mineralization. *Min. Resourc. Geol.* 26, 95–100 (in Chinese with English abstract).
- Li, W.B., Huang, Z.L., Chen, J., Han, R.S., Zhang, Z.L., Xu, C., 2004. Rb-Sr dating of mineral assemblage from the Huize giant Zn-Pb deposit, Yunnan Province. *Acta Petrol. Sin.* 24, 112–116 (in Chinese with English abstract).
- Li, W.B., Huang, Z.L., Yin, M.D., 2007. Dating of the giant Huize Zn-Pb ore field of Yunnan Province, southwest China: Constraints from the Sm-Nd system in hydrothermal calcite. *Resour. Geol.* 57, 90–97.
- Lin, Z.Y., Wang, D.H., Zhang, C.Q., 2010. Rb-Sr isotopic age of sphalerite from the Paoma lead-zinc deposit in Sichuan Province and its implications. *Geol. China* 37, 488–494.
- Liu, H.C., Lin, W.D., 1999. Regularity research of lead-zinc-silver deposits in northeastern Yunnan Province. Yunnan University Press, Kunming, pp 1–468 (in Chinese).
- Luo, K., Zhou, J.X., Huang, Z.L., Wang, X.C., Wilde, S.A., Zhou, W., Tian, L., 2019. New insights into the origin of early Cambrian carbonate-hosted Pb-Zn deposits in South China: A case study of the Maliping Pb-Zn deposit. *Gondwana Res.* 70, 88–103.
- Maréchal, C.N., Sheppard, S.M.F., 2002. Isotopic fractionation of Cu and Zn between chloride and nitrate solutions and malachite or smithsonite at 30°C and 50°C Goldschmidt Conference. *Geochim. Cosmochim. Acta* 66, A484.
- Mason, T.F.D., Weiss, D.J., Chapman, J.B., Wilkinson, J.J., Tessalina, S.G., Spiro, B., Horstwood, M.S.A., Spratt, J., Coles, B.J., 2005. Zn and Cu isotopic variability in the Alexandrinka volcanic-hosted massive sulfide (VHMS) ore deposit, Urals, Russia. *Chem. Geol.* 221, 170–187.
- Moynier, F., Vance, D., Fujii, T., Savage, P., 2017. The isotope geochemistry of zinc and copper. *Rev. Mineral. Geochim.* 82, 543–600.
- Pašava, J., Tornos, F., Chrástný, V., 2014. Zinc and sulfur isotope variation in sphalerite from carbonate-hosted zinc deposits, Cantabria, Spain. *Miner. Depos.* 49, 797–807.
- Ostendorf, J., Henjes-Kunst, F., Schneider, J., Melcher, F., Gutzmer, J., 2017. Genesis of the carbonate-hosted Tres Marias Zn-Pb-(Ge) deposit, Mexico: Constraints from Rb-Sr sphalerite geochronology and Pb isotopes. *Econ. Geol.* 112, 1075–1087.
- Qiu, L., Yan, D.P., Tang, S.L., Wang, Q., Yang, W.X., Tang, X.L., Wang, J.B., 2016. Mesozoic geology of southwestern China: Indosinian foreland overthrusting and subsequent deformation. *J. Asian Earth Sci.* 122, 91–105.
- Ren, S.L., Li, Y.H., Zeng, P.S., Qiu, W.L., Fan, C.F., Hu, G.Y., 2018. Effect of sulfate evaporate salt layer in mineralization of the Huize and Maoping lead-zinc deposits in Yunnan: Evidence from sulfur isotope. *Acta Geol. Sin.* 92, 1041–1055 (in Chinese with English abstract).
- Rosa, D., Schneider, J., Chiaradia, M., 2016. Timing and metal sources for carbonate-hosted Zn-Pb mineralization in the Franklinian Basin (North Greenland): Constraints from Rb-Sr and Pb isotopes. *Ore Geol. Rev.* 79, 392–407.
- Schwartz, M.O., 2000. Cadmium in zinc deposits: Economic geology of a polluting element. *Int. Geol. Rev.* 42, 445–469.
- Tan, S.C., Zhou, J.X., Luo, K., Xiang, Z.Z., He, H.H., Zhang, Y.H., 2019. The sources of ore-forming elements of the Maoping Large-Scale Pb-Zn deposit, Yunnan Province: Constraints from in situ S and Pb isotopes. *Acta Petrol. Sin.* 35, 3461–3476 (in Chinese with English abstract).
- Tang, Y.Y., Bi, X.W., Zhou, J.X., Liang, F., Qi, Y.Q., Leng, C.B., Zhang, X.C., Zhang, H., 2019. Rb-Sr isotopic age, S-Pb-Sr isotopic compositions and genesis of the ca. 200 Ma Yunluheba Pb-Zn deposit in NW Guizhou Province, SW China. *J. Asian Earth Sci.* 185, 104054.
- Tang, S.H., Zhu, X.K., Cai, J.J., Li, S.Z., He, X.X., Wang, J.H., 2006. Chromatographic separation of Cu, Fe and Zn using AGMP-1 anion exchange resin for isotope determination by MC-ICPMS. *Rock Min. Anal.* 25, 5–8 (in Chinese with English abstract).
- Wang, C.W., Yuan, L.I., Luo, H.Y., Liu, X.L., 2009. Genesis of Maoping Pb-Zn deposit in Yunnan province. *J. Kunming Univ. Sci. Technol.* 34, 7–11 (in Chinese with English abstract).
- Wang, Y.J., Fan, W.M., Zhang, G.W., Zhang, Y.H., 2013. Phanerozoic tectonics of the South China Block: Key observations and controversies. *Gondwana Res.* 23, 1273–1305.
- Wang, Z.Z., Liu, S.A., Liu, J., Huang, J., Xiao, Y., Chu, Z.Y., Zhao, X.M., Tang, L.M., 2017. Zinc isotope fractionation during mantle melting and constraints on the Zn isotope composition of Earth's upper mantle. *Geochim. Cosmochim. Acta* 198, 151–167.
- Wei, A.Y., Xue, C.D., Hong, T., Luo, D.F., Li, L.R., Wang, F., Zhou, G.M., Liu, X., 2012. The alteration-mineralization zoning model for the Maoping lead-zinc deposit, northeastern Yunnan Province: Evidence from alteration-lithofacies mapping. *Acta Petrologica et Mineralogica* 5, 723–735 (in Chinese with English abstract).
- Wei, A.Y., Xue, C.D., Xiang, K., Li, J., Liao, C., Akhter, Q.J., 2015. The ore-forming process of the Maoping Pb-Zn deposit, northeastern Yunnan, China: Constraints from cathodoluminescence (CL) petrography of hydrothermal dolomite. *Ore Geol. Rev.* 70, 562–577.
- Wei, C., Ye, L., Li, Z.L., Hu, Y.S., Huang, Z.L., Liu, Y.P., Wang, H.Y., 2020. Metals sources and ore genesis of the Wusihé Pb-Zn deposit in Sichuan, China: New evidence from in-situ S and Pb isotopes. *Acta Petrol. Sin.* 36 (12), 3783–3796 (in Chinese with English abstract).
- Wei, C., Ye, L., Hu, Y.S., Huang, Z.L., Danyushevsky, L., Wang, H.Y., 2021. LA-ICP-MS analyses of trace elements in base metal sulfides from carbonate-hosted Zn-Pb deposits, South China: A case study of the Maoping deposit. *Ore Geol. Rev.*, DOI: <https://doi.org/10.1016/j.oregeorev.2020.103945>.
- Wen, H.J., Zhu, C.W., Zhang, Y.X., Cloquet, C., Fan, H.F., Fu, S.H., 2016. Zn/Cd ratios and cadmium isotope evidence for the classification of lead-zinc deposits. *Sci. Rep.* 6, 25273.
- Wilkinson, J.J., Weiss, D.J., Mason, T.F.D., Coles, B.J., 2005. Zinc isotope variation in hydrothermal systems: Preliminary evidence from the Irish Midlands ore field. *Econ. Geol.* 100, 583–590.
- Wu, T., Huang, Z.L., Ye, L., Wei, C., Chen, J., Yang, M., Yan, Z.F., Sui, Z.H., 2020. Origin of the carbonate-hosted Danaopo Zn-Pb deposit in western Hunan Province, China: Geology and in-situ mineral S-Pb isotope constraints. *Ore Geol. Rev.*, DOI: <https://doi.org/10.1016/j.oregeorev.2020.103941>.
- Wu, Y., 2013. The age and ore-forming process of MVT deposits in the boundary area of Sichuan-Yunnan-Guizhou provinces, Southwest China. Ph.D. dissertation. Chinese University of Geosciences, Beijing, pp. 12–151 (in Chinese with English abstract).
- Xiang, Z.Z., Zhou, J.X., Luo, K., 2020. New insights into the multi-layer metallogenesis of carbonated-hosted epigenetic Pb-Zn deposits: A case study of the Maoping Pb-Zn deposit, South China. *Ore Geology Reviews*, doi.org/10.1016/j.oregeorev.2020.103538.
- Xu, C., Zhong, H., Hu, R.Z., Wen, H.J., Zhu, W.G., Bai, Z.J., Fan, H.F., Li, F.F., Zhou, T., 2019. Sources and ore-forming fluid pathways of carbonate-hosted Pb-Zn deposits in Southwest China: Implications of Pb-Zn-S-Cd isotopic compositions. *Miner. Depos.* 55, 491–513.
- Xu, Y., Chung, S.L., Jahn, B.M., Wu, G., 2001. Petrologic and geochemical constraints on the petrogenesis of Permian-Triassic Emeishan flood basalts in southwestern China. *Lithos* 58, 145–168.
- Yan, D.P., Zhou, M.F., Song, H.L., Fu, Z.R., 2003. Structural style and tectonic significance of the Jianglang dome in the eastern margin of the Tibetan Plateau, China. *J. Struct. Geol.* 25, 765–779.
- Yang, J.L., Li, Y.B., Liu, S.Q., Tian, H.Q., Chen, C.Y., Liu, J.M., Shi, Y.L., 2015. Theoretical calculations of Cd isotope fractionation in hydrothermal fluids. *Chem. Geol.* 391, 74–82.
- Yang, Q., Liu, W., Zhang, J., Wang, J., Zhang, X., 2019. Formation of Pb-Zn deposits in the Sichuan-Yunnan-Guizhou triangle linked to the Youjiang foreland basin: evidence from Rb-Sr age and in situ sulfur isotope analysis of the Maoping Pb-Zn deposit in northeastern Yunnan Province, southeast China. *Ore Geol. Rev.* 107, 780–800.
- Yang, Y.H., Zhang, X.C., Liu, S.A., Zhou, T., Fan, H.F., Yu, H.M., Cheng, W.H., Huang, F., 2018. Calibrating NIST SRM 683 as a new international reference standard for Zn isotopes. *J. Anal. At. Spectrom.* 33, 1777–1783.
- Yuan, H.L., Yuan, W.T., Cheng, C., Liang, P., Liu, X., Dai, M.N., Bao, Z., Zong, C.L., Chen, K.Y., Lai, S.C., 2016. Evaluation of lead isotope compositions of NIST NBS 981 measured by thermal ionization mass spectrometer and multiple-collector inductively coupled plasma mass spectrometer. *Solid Earth Sci.* 1, 74–78.
- Zartman, R.E., Doe, B.R., 1981. Plumbotectonics-the model. *Tectonophysics* 75, 135–162.
- Zhang, C.Q., Wu, Y., Hou, L., Mao, J.W., 2015. Geodynamic setting of mineralization of Mississippi Valley-type deposits in world-class Sichuan-Yunnan-Guizhou Zn-Pb triangle, southwest China: Implications from age-dating studies in the past decade and the Sm-Nd age of the Jinshachang deposit. *J. Asian Earth Sci.* 103, 103–114.
- Zhang, H.J., Fan, H.F., Xiao, C.Y., Wen, H.J., Zhu, X.K., Ye, L., Huang, Z.L., Zhou, J.X., 2019a. Homogeneous Zn isotopic compositions in the Maozu Zn-Pb ore deposit in Yunnan Province, southwestern China. *Ore Geol. Rev.* 109, 1–10.
- Zhang, H.J., Fan, H.F., Xiao, C.Y., Wen, H.J., Ye, L., Huang, Z.L., Zhou, J.X., Guo, Q.J., 2019b. The mixing of multi-source fluids in the Wusihé Zn-Pb ore deposit in Sichuan Province, Southwestern China. *Acta Geochim.* 38, 642–653.
- Zhang, Y.X., Wen, H.J., Zhu, C.W., Fan, H.F., Luo, C.G., Liu, J., Cloquet, C., 2016. Cd isotope fractionation during simulated and natural weathering. *Environ. Pollut.* 216, 9–17.
- Zhao, X.F., Zhou, M.F., Li, J.W., Sun, M., Gao, J.F., Sun, W.H., Yang, J.H., 2010. Late Paleoproterozoic to early Mesoproterozoic Dongchuan Group in Yunnan, SW China: Implications for tectonic evolution of the Yangtze Block. *Precambr. Res.* 182, 57–69.
- Zhou, J.X., Huang, Z.L., Zhou, M.F., Li, X.B., Jin, Z.G., 2013a. Constraints of C-O-S-Pb isotope compositions and Rb-Sr isotopic age on the origin of the Tianqiao carbonate-hosted Pb-Zn deposit, SW China. *Ore Geol. Rev.* 53, 77–92.
- Zhou, J.X., Huang, Z.L., Yan, Z.F., 2013b. The origin of the Maozu carbonate-hosted Pb-Zn deposit, southwest China: Constrained by C-O-S-Pb isotopic compositions and Sm-Nd isotopic age. *J. Asian Earth Sci.* 73, 39–47.
- Zhou, J.X., Huang, Z.L., Zhou, M.F., Zhu, X.K., Muchez, P., 2014a. Zinc, sulfur and lead isotopic variations in carbonate-hosted Pb-Zn sulfide deposits, southwest China. *Ore Geol. Rev.* 58, 41–54.
- Zhou, J.X., Huang, Z.L., Lv, Z.C., Zhu, X.K., Gao, J.G., Mirnejad, H., 2014b. Geology, isotope geochemistry and ore genesis of the Shanshulin carbonate-hosted Pb-Zn deposit, southwest China. *Ore Geol. Rev.* 63, 209–225.
- Zhou, J.X., Bai, J.H., Huang, Z.L., Zhu, D., Yan, Z.F., Lv, Z.C., 2015. Geology, isotope geochemistry and geochronology of the Jinshachang carbonate-hosted Pb-Zn deposit, southwest China. *J. Asian Earth Sci.* 98, 272–284.
- Zhou, J.X., Luo, K., Wang, X.C., Wilde, S.A., Wu, T., Huang, Z.L., Cui, Y.L., Zhao, J.X., 2018a. Ore genesis of the Fule Pb-Zn deposit and its relationship with the Emeishan Large Igneous Province: Evidence from mineralogy, bulk C-O-S and in situ S-Pb isotopes. *Gondwana Res.* 54, 161–179.
- Zhou, J.X., Xiang, Z.Z., Zhou, M.F., Feng, Y.X., Luo, K., Huang, Z.L., Wu, T., 2018b. The giant Upper Yangtze Pb-Zn province in SW China: Reviews, new advances and a new genetic model. *J. Asian Earth Sci.* 154, 280–315.
- Zhou, M.F., Malpas, J., Song, X.Y., Robinson, P.T., Sun, M., Kennedy, A.K., Esher, C.M., Keays, R.R., 2002. A temporal link between the Emeishan large igneous province

- (SW China) and the end Guadalupian mass extinction. *Earth Planet Sci. Lett.* 196, 113–122.
- Zhu, C.W., Wen, H.J., Zhang, Y.X., Fan, H.F., Fu, S.H., Xu, J., Qin, T.R., 2013. Characteristics of Cd isotopic compositions and their genetic significance in the lead-zinc deposits of SW China. *Sci. China-Earth Sci.* 56, 2056–2065.
- Zhu, C.W., 2014. Geochemistry of Cd and Ge, and their isotopes in Carbonate-hosted lead-zinc ore deposits in the boundary area of Sichuan, Yunnan and Guizhou Provinces, China. Ph.D. dissertation. Institute of Geochemistry, Chinese Academy of Sciences, Guiyang 1–123 (in Chinese with English abstract).
- Zhu, C.W., Wen, H.J., Zhang, Y.X., Fu, S.H., Fan, H.F., Cloquet, C., 2016. Cadmium isotope fractionation in the Fule Mississippi Valley-type deposit, Southwest China. *Miner. Depos.* 52, 675–686.
- Zhu, C.W., Liao, S.L., Wang, W., Zhang, Y.X., Yang, T., Fan, H.F., Wen, H.J., 2018. Variations in Zn and S isotope chemistry of sedimentary sphalerite, Wusihe Zn-Pb deposit, Sichuan Province, China. *Ore Geol. Rev.* 95, 639–648.
- Zhu, C.W., Wen, H.J., Wang, J., Zhang, J.W., Chen, X.C., Fan, H.F., Zhang, Y.X., Yang, T., 2020. Isotope geochemistry of Zn, Pb and S in the Ediacaran strata hosted Zn-Pb deposits in Southwest China. *Ore Geol. Rev.* 117, 1–10.
- Zhu, X.K., Guo, Y., Williams, R.J.P., O'Nions, R.K., Matthews, A., Belshaw, N.S., Canters, G.W., De, W.E.C., Weser, U., Burgess, B.K., Salvato, B., 2002. Mass fractionation processes of transition metal isotopes. *Earth Planet Sci. Lett.* 200, 47–62.